REPORT NO.
UCB/SEMM-89/09

STRUCTURAL ENGINEERING,
MECHANICS AND MATERIALS

PLATE BENDING ELEMENTS WITH DISCRETE CONSTRAINTS: NEW TRIANGULAR ELEMENTS

by

O. C. ZIENKIEWICZ, R. L. TAYLOR,
P. PAPADOPOULOS and E. ONATE

MARCH 1989

DEPARTMENT OF CIVIL ENGINEERING
UNIVERSITY OF CALIFORNIA AT BERKELEY
BERKELEY, CALIFORNIA

PLATE BENDING ELEMENTS WITH DISCRETE CONSTRAINTS: NEW TRIANGULAR ELEMENTS

O. C. Zienkiewicz [1], *R. L. Taylor* [2],
P. Papadopoulos [2] *and E. Oñate* [3]

ABSTRACT

In recent years a series of elements based on Reissner-Mindlin assumptions and using discrete (collocation type) constraints have been introduced. These elements have proved to be very effective - but their relation to straight-forward mixed approximations was not clear. In this paper this relationship is discussed and the reasons for their success explained. This allows new and effective triangular elements to be developed.

The presentation shows the close relationships with the DKT (Discrete Kirchhoff Theory) element previously available only for thin plates and allows extension of their applications.

1. Introduction

The problem of plate bending was one of the first tackled by the finite element method in the early sixties and yet today is still subject to much research, designed to improve the performance of bending elements. The subject is of much importance in structural engineering and satisfactory solutions of plate bending behavior form a necessary prerequisite for the analysis of shells.

The original approaches invariably utilized the thin plate, Kirchhoff, theory used in a direct (irreducible) manner and immediately encountered the difficulties of imposing the C^1 continuity of shape functions necessary for the finite element formulation. Later work approached plates directly as an approximation to three dimensional analysis [1,2], or, which is equivalent, by the use of the Reissner [30] - Mindlin [22], *thick* plate, theory. This by-passed the difficulties caused by the C^1 requirement but introduced its own problems immediately. In particular locking behavior was observed as the thickness was reduced and various artifices had to be used to eliminate such effects. The most successful of these was the introduction of *reduced* or *selective* integration procedures [18,21,26,27,42]. However, even this was not generally sufficient and almost all elements of that type proved non-robust, failing under diverse circumstances. Other approaches have also been proposed, including use of incompatible modes in the description of the transverse shear strain [25].

[1] Institute for Numerical Methods in Engineering, University of Wales, Swansea, U.K.
[2] Department of Civil Engineering, University of California at Berkeley, Berkeley, CA, USA.
[3] E.T.S. Ingenieros de Caminos, Canales, y Puertos, Universidad Politécnica de Cataluña, Barcelona, Spain

The thick plate theory can of course be used as a basis for a mixed finite element approximation if shear forces and displacements are approximated independently. Indeed, the realization of this led Malkus and Hughes [21] to demonstrate the equivalence of selective integration with a penalized version of the mixed form. More recently a fuller analysis [40] of the mixed formulation which is, of course, valid for both 'thick' and 'thin' plates indicated why the failure of 'thick' forms occurs frequently in practice. Indeed, this analysis showed how successful elements could be developed and the first fully robust element based on the direct Reissner-Mindlin approach was introduced only very recently [41].

Since 1981, however, a very successful approach to the formulation of elements based on the 'thick' theory was developed using *smoothed shear strain fields* and concentrated, discrete, constraints [6,14-16,19]. The relationship of this approach to direct, mixed, approximation was however not clear (at least to the present authors) and in particular it was not evident why such elements should be exempt from the various convergence criteria given in reference 40. In this paper we shall attempt to

(a) present a comprehensive explanation of various mixed and direct approximations, and

(b) show how the procedures can be applied to development of new plate elements generally - and to a triangle in particular.

While the proponents of the thick plate, Mindlin-Reissner, approach were overcoming the difficulties mentioned above, those approaching the formulation via the Kirchhoff theory successfully avoided the C^1 continuity requirements, by imposing the Kirchhoff constraints in a 'discrete manner' (often referred to as a Discrete Kirchhoff Theory). The concepts were first introduced as early as 1968 [36] by Wempner et. al., but the development of successful elements by this procedure has been continuous up to the present date. References 5, 7-10, 12, 13, 24, 32, 39 list some of the salient stages of this story. It is evident that this direction of progress, which we shall term DKT for short, must be related to the full mixed formulation with discrete constraints and we shall discuss this relationship here. This proves indeed to be correct and hence a more unified view of the plate problems can now emerge.

Before proceeding with the main topic of the paper we would like to point out to the reader that the fields of applicability of thick and thin plate approximations are by no means always obvious. Very recently Babuska and Scapolla [4] showed how in an apparently very thin plate (thickness/span equal 0.01), errors of circa 5% in displacements can occur between the true behavior and that predicted on the basis of Kirchhoff hypotheses. For this reason the approaches based *a priori* on thick plate equations, but which are capable of representing thin forms, are optimal. It is with such methods that we are here concerned.

2. The background theory

The *thick*, Reissner-Mindlin, theory of plates introduces two assumptions which are physically plausible when the thickness is small compared to other dimensions.

- The first assumption is that the normals to the mid-surface of the plate before deformation remain straight after deformation (but do not necessarily remain normal to it).
- The second assumption is that the stresses normal to the mid-plane direction (and indeed their effects) remain negligible.

With these assumptions it is possible to describe all displacements in the plate by the knowledge of the rotations and displacements of the mid-plane of the plate.

We can thus write

$$u = z\,\theta_x(x,y) \quad ; \quad v = z\,\theta_y(x,y) \quad ; \quad w = w(x,y) \tag{1}$$

where θ_x , θ_y and w are dependent only on the two in plane coordinates x , y, Fig. 1, and z is the direction normal to it.

The strains in the plate are thus, for planes parallel to x , y, given by the following

$$\epsilon_x = z\,\frac{\partial\theta_x}{\partial x} \quad ; \quad \epsilon_y = z\,\frac{\partial\theta_y}{\partial y} \quad ; \quad \gamma_{xy} = z\,[\,\frac{\partial\theta_x}{\partial y} + \frac{\partial\theta_y}{\partial x}\,] \tag{2}$$

and in the vertical direction

$$\gamma_{xz} = [\,\theta_x + \frac{\partial w}{\partial x}\,] \quad ; \quad \gamma_{yz} = [\,\theta_y + \frac{\partial w}{\partial y}\,] \tag{3}$$

Constitutive relations allow all stresses and hence stress resultants to be evaluated. For isotropic, homogeneous, elasticity we have for the bending moments defined below

$$M_x = \int_{-\frac{t}{2}}^{\frac{t}{2}} \sigma_x \, z \, dz \quad ; \quad M_y = \int_{-\frac{t}{2}}^{\frac{t}{2}} \sigma_y \, z \, dz \quad ; \quad M_{xy} = \int_{-\frac{t}{2}}^{\frac{t}{2}} \sigma_{xy} \, z \, dz \tag{4}$$

and the following relations

$$\mathbf{M} = \mathbf{D}\mathbf{L}\boldsymbol{\theta} \quad ; \quad \mathbf{D} = \frac{E\,t^3}{12(1-\nu^2)} \begin{bmatrix} 1 & \nu & 0 \\ \nu & 1 & 0 \\ 0 & 0 & \frac{1-\nu}{2} \end{bmatrix} \tag{5}$$

Here E and ν are the elastic modulus and Poisson's ratio, t the plate thickness and

$$\mathbf{M}^T = [M_x, M_y, M_{xy}] \tag{6}$$

$$\boldsymbol{\theta}^T = [\theta_x, \theta_y]$$

The operator $\mathbf{L}$ follows from (2) as

$$\mathbf{L} = \begin{bmatrix} \frac{\partial}{\partial x} & 0 \\ 0 & \frac{\partial}{\partial y} \\ \frac{\partial}{\partial y} & \frac{\partial}{\partial x} \end{bmatrix} \tag{7}$$

Similarly the transverse shear forces are defined by

$$S_x = \int_{-\frac{t}{2}}^{\frac{t}{2}} \tau_{xz} \, dz \quad ; \quad S_y = \int_{-\frac{t}{2}}^{\frac{t}{2}} \tau_{yz} \, dz \tag{8}$$

and the constitutive relation is

$$\mathbf{S} = \alpha[\boldsymbol{\theta} + \nabla w] \quad ; \quad \alpha = \kappa G\, t \tag{9}$$

Here G is the shear modulus of the material and κ a factor which depends on the plate properties (a commonly used value of κ is $\frac{5}{6}$).

To the above relations two equilibrium equations need to be added. The first relates the bending moments to shear forces and is simply

$$\mathbf{L}^T\mathbf{M} + \mathbf{S} = \mathbf{0} \tag{10}$$

The second is a statement of lateral equilibrium

$$\nabla^T \mathbf{S} + q = 0 \tag{11}$$

Various possibilities exist regarding the choice of variables to be retained in the final equation system when approximation is to be made. We shall here retain w, $\boldsymbol{\theta}$, and $\mathbf{S}$ and write the system as

$$\mathbf{L}^T \mathbf{D} \mathbf{L} \boldsymbol{\theta} + \mathbf{S} = \mathbf{0} \tag{12a}$$

From (9),

$$\frac{1}{\alpha}\mathbf{S} - (\boldsymbol{\theta} + \nabla w) = \mathbf{0} \tag{12b}$$

and repeating (11)

$$\nabla^T \mathbf{S} + q = 0 \tag{12c}$$

The equation system forms the basis of a *mixed formulation* if $\boldsymbol{\theta}$, w and $\mathbf{S}$ are approximated independently. The *thin* plate, Kirchhoff, approximation is simply a limiting case in which $\alpha = \infty$ and (12b) is then the well known constraint

$$\boldsymbol{\theta} + \nabla w = \mathbf{0} \tag{13}$$

This ensures that during deformation the normals remain normal to the middle plane of the plate.

The formulation by (12) is *mixed* as it is possible to eliminate one of the variables, $\mathbf{S}$ by use of (12b), from the system when an irreducible form is obtained. The latter is indeed the basis from which most thick plate approximations start but as a finite value of α is needed to perform the elimination such forms are not available for the thin plate limit.[3]

It is generally anticipated, however, that the thin plate behavior will be approximated to as α becomes progressively larger and goes to infinity. However, this is not true in most finite element approximations unless the equivalent mixed form of (12) is solvable. If it is not, singularities and/or locking will occur.

The equation system (12) is frequently interpreted as a minimization of total potential energy defined as [37]

---

[3] It is of course possible to eliminate $\mathbf{S}$ and $\boldsymbol{\theta}$ even if α is infinite using appropriate differentiation. This leads to the biharmonic thin plate equations.

$$\Pi = \tfrac{1}{2}\int_{\Omega} (\mathbf{L}\,\theta)^T \mathbf{D} (\mathbf{L}\,\theta)\, d\Omega + \tfrac{1}{2}\int_{\Omega} \mathbf{S}^T \alpha^{-1} \mathbf{S}\, d\Omega - \int_{\Omega} w\, q\, d\Omega \tag{14a}$$

subject to the constraints given by (12b), i.e.,

$$\frac{1}{\alpha}\mathbf{S} = (\theta + \nabla w) \tag{14b}$$

This constraint, if directly eliminated at the above level, leads to a standard penalized form which we discussed above; if the constraint is incorporated in a new functional by means of a Lagrangian multiplier we shall find the well known Hellinger-Reissner variational theorem, etc.

Other possibilities exist in the solution as we show in the next section.

3. The finite element approximation to the mixed form

If we wish to retain a solution capable of covering the full *thick* and *thin* range (i.e., not failing when $\alpha = \infty$), it is necessary to approximate all the variables and write [4]

$$\theta = \mathbf{N}_\theta \bar{\theta} \quad ; \quad w = \mathbf{N}_w \bar{w} \quad ; \quad \mathbf{S} = \mathbf{N}_S \bar{\mathbf{S}} \tag{15}$$

In the above $\mathbf{N}_\theta$, $\mathbf{N}_w$ and $\mathbf{N}_S$ stand for the appropriate shape functions in the x , y domain, and $\bar{\theta}$, $\bar{w}$ and $\bar{\mathbf{S}}$ are the associated (nodal) parameters.

All possible approximations can be obtained using suitable weighting functions [39] on the equation system (12) and the resulting equation will always be of the type

$$\begin{bmatrix} \mathbf{A} & \mathbf{B} & \mathbf{0} \\ \bar{\mathbf{B}}^T & \mathbf{H}/\alpha & \mathbf{C} \\ \mathbf{0} & \bar{\mathbf{C}}^T & \mathbf{0} \end{bmatrix} \begin{Bmatrix} \bar{\theta} \\ \bar{\mathbf{S}} \\ \bar{w} \end{Bmatrix} = \begin{Bmatrix} \mathbf{f}_1 \\ \mathbf{f}_2 \\ \mathbf{f}_3 \end{Bmatrix} \tag{16}$$

In the particular case of the approximation arising via the variational principle the above equation will be symmetric but this is not always necessarily so.

In another paper (reference 40) we have shown that it is necessary, if an algebraic solution of the system of equation (16) in the limiting case when $\alpha = \infty$ is possible, to satisfy

$$n_\theta + n_w \geq n_S \tag{17}$$

[4] More general interpolation may be used. For example we could write $w = \mathbf{N}_w \bar{w} + \mathbf{N}_{w\theta} \bar{\theta}$ so that displacements for transverse displacements involve parameters of the rotation. This is the form that the thin plate solution uses where the transverse displacement interpolation involves nodal parameters of displacement and rotations (e.g., Hermite interpolations). This type of interpolation also results from application of constraints [34].

$$n_S \geq n_w$$

where n_θ, n_w and n_S stand for the number of variables in each set of parameters $\bar{\theta}$, $\bar{w}$ and $\bar{S}$, respectively.

The above inequalities have to be satisfied also for various element patches as a condition which is necessary (although not always sufficient) for convergence [33,43].

In reference 40 we have examined a number of currently used elements and found that all failed this stringent test. Indeed only the element of reference 10 and an element introduced more recently by Arnold and Falk [3] satisfy the above count requirements and indeed converge in all circumstances. In Fig. 2 we show both these elements in a single element patch test in which displacements on the boundary are either fully constrained (Test C) or relaxed to a minimum restraining only the rigid body modes (Test R). In both cases these tests are satisfactorily passed and the reader can verify that the same occurs in larger element assemblies.

4. The discrete approximation on element boundaries

The elements developed by Bathe and Dvorkin [6,14] and Hinton and Huang [15,16] fall into the general category we have just discussed, but use a very special shear resultant interpolation. [5]

The first element of this series is a bilinear quadrilateral, or its special form the bilinear rectangle illustrated in Fig. 3. Here S is specified by interpolating S_x and S_y components separately in the manner shown.

If the substitution of above interpolation is made in a general formulation obtainable from the Hellinger-Reissner variational principle (or indeed using the standard Galerkin weighting approximation) we see immediately that the fully restrained patch test on a single element fails (as indeed does the test on element assemblies).

Now $n_\theta = 0$, $n_S = 4$ and $n_w = 0$ as shown in the figure noting that the parameters $\bar{S}$ are not restrained. Indeed the patch test will fail even more dramatically if an assembly of elements is con-

[5] In fact the interpolation is not for the shear resultants but for the quantity $S/\alpha = \gamma$ = shear strain. Results however will still be identical if α is assumed constant.

sidered as shown in Fig. 4.

Difficulties can however be overcome by the use of *discrete*, collocation type, approximations to equation (12b). If the equation appropriate to a particular component is satisfied at a single point of the side (by using Dirac delta weighting) we can write for such a point as A placed in the middle of side 1-2 of Fig. 3

$$\frac{1}{\alpha}S_y = \frac{1}{\alpha}\bar{S}_y = \theta_y + \frac{\partial w}{\partial y} = \frac{\bar{\theta}_y^1 + \bar{\theta}_y^2}{2} + \frac{\bar{w}^2 - \bar{w}^1}{h} \tag{18}$$

with three similar equation on other sides.

This immediately ensures that $\bar{S}_y$ is explicitly determined by the two end values of $\bar{\theta}$ and $\bar{w}$ and that their prescription uniquely determines $\bar{S}_y$ values. On boundaries these are therefore no longer free parameters to be taken into account in the patch test. Now for the single element test $n_S = 0$ and the patch count is passed.

Indeed the unique specification of $\bar{S}_y$ by the end values means at element interfaces such as shown in Fig. 4 only a single value of $\bar{S}_y$ (or $\bar{S}_x$) is a free parameter. In that figure we show that the patch test, though not yet completely passed, is much more closely approximated.

The idea can of course be extended to include more variables as shown by Hinton and Huang [15,16]. In their element, with bi-quadratic θ and w approximation, each of the shear components is interpolated by placing two nodes on the appropriate sides as shown in Fig. 5. Though additional parameters (and collocation points) are placed in the interior of the element, the parameters on interfaces are uniquely defined by the $\bar{\theta}$ and $\bar{w}$ lying on those faces and thus are constrained fully on the boundary. This formulation fails the test for a single element but passes the test for multiple assemblies and is more robust than the Bathe-Dvorkin version.

It should be noted that point collocation is of course not the only way to ensure the desired effect. Any weighting specified only on the element boundaries will suffice to achieve this. For instance requiring that in the previous example we have

$$\int_1^2 [\frac{1}{\alpha}S_y - \theta_y - \frac{\partial w}{\partial y}] d\Gamma = 0 \tag{19}$$

or indeed specifying collocation points not placed at the center of an element boundary will be satisfactory though not necessarily equally accurate. Results given in Section 7 are for a triangular element which has shear constraints expressed in the form of (19).

5. Element stiffness matrices

The discrete constraint equations approximating to (12b) can be written as

$$\frac{1}{\alpha}\bar{\mathbf{S}} = \mathbf{Q}\begin{Bmatrix}\bar{\boldsymbol{\theta}}\\ \bar{\mathbf{w}}\end{Bmatrix} = \mathbf{Q}_\theta\,\bar{\boldsymbol{\theta}} + \mathbf{Q}_w\,\bar{\mathbf{w}} \tag{20}$$

providing the number of constraint relationships is equal to that of the number of variables S. Here Q is an easily found matrix and this allows the variables S to be eliminated from (12a) and (12c). These in turn can be discretized by appropriate weighting. However it is difficult *a priori* to determine the weighting which will result in symmetric stiffness matrices and for this reason it is convenient to return to the variational form given by (14a,b).

Now the variational function of (14a) can be written in a discrete form and (20), together with the shear approximations, may be used to eliminate S.

We can thus insert into (14a) [6]

$$\boldsymbol{\theta} = \mathbf{N}_\theta\,\bar{\boldsymbol{\theta}} \quad ; \quad w = \mathbf{N}_w\,\bar{\mathbf{w}} \tag{21a}$$

and

$$\mathbf{S} = \mathbf{N}_S\,\bar{\mathbf{S}} = \alpha\,\mathbf{N}_S\,[\mathbf{Q}_\theta\,\bar{\boldsymbol{\theta}} + \mathbf{Q}_w\,\bar{\mathbf{w}}] \tag{21b}$$

and minimize appropriately with respect to the parameters $\bar{\boldsymbol{\theta}}$ and $\bar{\mathbf{w}}$.

On insertion of the above into the functional we have immediately

$$\begin{aligned}\Pi = {} & \tfrac{1}{2}\int_\Omega [\mathbf{L}\,\mathbf{N}_\theta\,\bar{\boldsymbol{\theta}}]^T\,\mathbf{D}\,[\mathbf{L}\,\mathbf{N}_\theta\,\bar{\boldsymbol{\theta}}]\,d\Omega\\ & + \tfrac{1}{2}\int_\Omega [\mathbf{N}_S\,\mathbf{Q}_\theta\,\bar{\boldsymbol{\theta}} + \mathbf{N}_S\,\mathbf{Q}_w\,\bar{\mathbf{w}}]^T\,\alpha\,[\mathbf{N}_S\,\mathbf{Q}_\theta\,\bar{\boldsymbol{\theta}} + \mathbf{N}_S\,\mathbf{Q}_w\,\bar{\mathbf{w}}]\,d\Omega\\ & - \int_\Omega [\mathbf{N}_w\,\bar{\mathbf{w}}]^T\,q\,d\Omega\end{aligned} \tag{22}$$

[6] Note that the interpolation for w may need to be generalized if it involves nodal parameters $\bar{\mathbf{w}}$ and $\bar{\boldsymbol{\theta}}$.

and on minimization we obtain

$$\begin{bmatrix} \mathbf{K}_{\theta\theta} & \mathbf{K}_{\theta w} \\ \mathbf{K}_{w\theta} & \mathbf{K}_{ww} \end{bmatrix} \begin{Bmatrix} \bar{\theta} \\ \bar{w} \end{Bmatrix} = \begin{Bmatrix} \mathbf{f}_1 \\ \mathbf{f}_2 \end{Bmatrix} \tag{23}$$

with

$$\mathbf{K}_{\theta\theta} = \int_{\Omega} [(\mathbf{L}\,\mathbf{N}_\theta)^T\,\mathbf{D}\,(\mathbf{L}\,\mathbf{N}_\theta) + (\mathbf{N}_S\,\mathbf{Q}_\theta)^T\,\alpha\,(\mathbf{N}_S\,\mathbf{Q}_\theta)]\,d\Omega$$

$$\mathbf{K}_{\theta w} = \int_{\Omega} (\mathbf{N}_S\,\mathbf{Q}_\theta)^T\,\alpha\,(\mathbf{N}_S\,\mathbf{Q}_w)\,d\Omega = \mathbf{K}_{w\theta}^T$$

$$\mathbf{K}_{ww} = \int_{\Omega} (\mathbf{N}_S\,\mathbf{Q}_w)^T\,\alpha\,(\mathbf{N}_S\,\mathbf{Q}_w)\,d\Omega$$

6. Oblique co-ordinates

The derivations of the preceding sections have been limited to simple rectangles and a direct interpolation of S_x and S_y shear components. Of course it is easy to generalize to curvilinear shapes using isoparametric or other mapped coordinates and to interpolate S_ξ and S_ζ in a similar way, defining

$$\frac{1}{\alpha} S_\xi = \theta_\xi + \frac{\partial w}{\partial \xi} \qquad etc. \tag{24}$$

Parameters defining $\bar{S_\xi}$ on element sides will now be necessary but the general algebra will be identical.[7] It will of course be necessary in the final computation to transfer the components to a Cartesian system - and we omit here the details which are adequately described in references [6,14-16,36].

7. New triangular elements

The concepts expounded in the previous section allow many new variants of *discretely constrained* elements to be derived. As an example we introduce three new triangles which are subsequently tested by applications to several example problems. Results from the tests are given in Section 9.

[7] In development of triangular elements we introduce tangential components along each edge which we shall refer to as θ_s and S_s.

7.1 Quadratic triangle - 6 node element

We consider first a triangle which is illustrated in Fig. 6. The interpolations for the transverse displacement, w, and rotation fields, θ, are assumed to vary quadratically over the element. Using hierarchical forms for the mid-side parameters the interpolations may be written as

$$\theta = \sum_{i=1}^{3} L_i \bar{\theta}^i + \sum_{i=1}^{3} 4 L_i L_j \Delta\bar{\theta}^k \tag{25}$$

and

$$w = \sum_{i=1}^{3} L_i \bar{w}^i + \sum_{i=1}^{3} 4 L_i L_j \Delta\bar{w}^k \tag{26}$$

where L_i are the standard area coordinates, $\Delta\bar{\theta}^k$ and $\Delta\bar{w}^k$ are hierarchical displacement and rotation parameters at the element mid-side,[8]

$$j = mod(i,3)+1 \quad ; \quad k = mod(j,3)+1$$

The interpolation for the transverse shear resultants is less obvious. Here six nodal values of shears parallel to the sides of the triangle and located at Gauss points as shown in Fig 6(a) uniquely define a linear distribution of shear resultants. Accordingly, we write first

$$\mathbf{S} = \sum_{i=1}^{3} L_i \bar{\mathbf{S}}^i \tag{27}$$

The coefficients $\bar{\mathbf{S}}^i$ can be uniquely determined by writing equations at the 6 constraint points and finally the full interpolation expression defining the shear resultant shape functions becomes

$$\mathbf{S} = \sum_{i=1}^{3} \frac{L_i}{\Delta_i} \begin{bmatrix} e_{ky} & -e_{jy} \\ -e_{kx} & e_{jx} \end{bmatrix} \begin{Bmatrix} g_1 \bar{S}_{j1} + g_2 \bar{S}_{j2} \\ g_2 \bar{S}_{k1} + g_1 \bar{S}_{k2} \end{Bmatrix} \tag{28}$$

where $\bar{S}_{j1}$ and $\bar{S}_{j2}$ are the tangential shear resultants at the 2-points on the j-edge,

$$g_1 = \frac{1}{2}(1-\sqrt{3}) \quad , \quad g_2 = \frac{1}{2}(1+\sqrt{3})$$

$$\Delta_i = e_{jx} e_{ky} - e_{jy} e_{kx}$$

In the above the components of $\mathbf{e}_j$ are the direction cosines of the sides on which $L_j = 0$. Fuller details of the derivation are given in Appendix A. A stiffness matrix for this element is computed

[8] The function $mod(i,j)$ is equal to $i-(i/j)*j$ where integer arithmetic is used evaluate i/j.

using (23) and in the numerical examples section the results are labeled TRI-6.

What is important to note is that at the mixed stage with variables $\bar{S}$ not eliminated all the counts of the mixed patch test are passed both in the single element and when several are assembled as shown in Fig. 7. Indeed on each edge there are but two shear constraints and there are 3 parameters at each mid-side. An element which still passes the patch test may be deduced by rotating the $\Delta\theta$ to normal and tangential directions and then constraining the $\Delta\theta_n = 0$ (i.e., the *normal* bending displacement component varies linearly on an edge while the *tangential* component varies quadratically). This element (called TRI-6R in the examples section) performs slightly better than the original element; however, it generally gives answers for displacements which are too large. In order to improve the performance further another modification is considered in the next part.

7.2 Linear/Quadratic triangle - 3 node element

In this formulation the rotation θ varies quadratically (although not all quadratic terms are present) within the element, according to the following interpolation [14], (Fig. 2)

$$\theta = \sum_{i=1}^{3} L_i \bar{\theta}^i + \sum_{i=1}^{3} 4 L_i L_j \Delta\bar{\theta}^k \mathbf{e}_k \tag{29}$$

where $\Delta\bar{\theta}^k$ is a hierarchical *tangential* rotation parameter at the element mid-side and j, k are as defined above. This is similar to the interpolations used in the formulation discussed above for the element called TRI-6R where the rotation normal to the element sides is assumed to vary linearly.

In addition, w is constrained to vary linearly over the element, according to

$$w = \sum_{i=1}^{3} L_i \bar{w}^i \tag{30}$$

The transverse shear resultant field again is assumed to be linear in each element and is expressed by (27). The $\bar{S}^i$ for this element are to be determined by satisfying discrete edge constraints which represent *constant* tangential shear resultant. This may be accomplished by using (28) and setting $\bar{S}_{j1}$ equal to $\bar{S}_{j2}$ and thus gives the three parameter interpolation

$$\mathbf{S} = \sum_{i=1}^{3} \frac{L_i}{\Delta_i} \begin{bmatrix} e_{ky} & -e_{jy} \\ -e_{kx} & e_{jx} \end{bmatrix} \begin{Bmatrix} \bar{S}_{j0} \\ \bar{S}_{k0} \end{Bmatrix} \tag{31}$$

where $\bar{S}_{j0}$ is the value of the constant tangential shear resultant on the j-edge. Fuller details are again contained in Appendix A. In the numerical examples section this element is called DRM (for Discrete Reissner-Mindlin) element as it is a direct generalization of the DKT triangle discussed in reference 16, 21, and 22.

The application of discrete collocation constants at the Gauss points of the sides, for either formulation above, results in the matrices $\mathbf{Q}_\theta$ and $\mathbf{Q}_w$ of (20) with details shown in Appendix B. The final determination of the stiffness matrices follows from expressions (22) and (23). Since both the bending and the transverse shear resultants vary linearly in each element, a three point Gauss quadrature results in an exact evaluation of all integrals (provided loading, q, is linearly interpolated over each element).

The above elements can be compared directly with another triangle derived in reference 10 and numerical tests, which we give later, show that they compare well. The derivation of the elements is simpler than that of [41] and we believe less costly. In some aspects the DRM element is similar to one proposed by Stolarski and Chiang [32], who however consider only the limiting thin plate situation.

8. Relation to DKT formulation

We have shown that the discrete constraints of the form of (2) when combined with the variational principles of (14a) and satisfying of the appropriate patch tests will converge to the thin plate solution. Indeed at that limit, when $\alpha = \infty$, we can drop the shear terms from the variational principle of (14a) and write the problem as minimization of

$$\Pi = \tfrac{1}{2}\int_{\Omega} (\mathbf{L}\,\theta)^T \mathbf{D} (\mathbf{L}\,\theta)\, d\Omega - \int_{\Omega} w\, q\, D\Omega \tag{32}$$

subject to discrete constraints (viz. (20))

$$\frac{1}{\alpha}\bar{\mathbf{S}} = \mathbf{Q}\begin{Bmatrix}\bar{\theta}\\ \bar{w}\end{Bmatrix} = \mathbf{0} \tag{33}$$

but no longer is any interpolation for S necessary.

The reader will observe that in fact, as mentioned in the previous section, our solution was simply a penalty form of the above problem. However other forms of imposing the constraints can be pursued.

One is the *direct substitution* of the constraints into the functional and thus the reduction of variables. This indeed is the procedure used by all DKT developers and is given in references 5, 7-10, 12, 13, 24, 32 and discussed in reference 39. We again note that the element described in section 7.2 leads to an expression which, when used in (33), gives immediately the DKT element described in references 7, 8, and 36 (for details see the Appendix). Another possibility is the use of *discrete Lagrangian parameters* to impose the constraints. This does not appear to have been done so far.

Both methods will give obviously identical results to those which represent the limit to which our discrete formulation will converge as $\alpha \to \infty$. The triangular DRM element we have discussed is therefore in the limit identical to the one in Fig. 8 in which the rotation has been eliminated along each side.

Indeed we can now determine the 'thick plate' equivalents of all (or at least most) of the elements presented in references 12, 20, 28, 29, 39. Of course the numerical results may depend on the manner in which the discrete constraints are imposed. As we have remarked already it is necessary to impose some of the constraints by point (or subdomain) collocation on the boundaries to reduce the constraints on element patches. However for parameters defined *inside* the element point collocation and/or an integral (area) weighting may be used. Providing this detail is identically treated in both approaches the limiting answers will be the same.

In Fig. 8 we show how the triangular element of reference 7 evolves. In Fig. 9 we show a series of rectangular (or quadrilateral) elements with discrete constraints based on the *thick plate* formulation developed here. The reader can verify that each of these satisfies the *patch test count* criteria for single and multiple element assemblies (Tests C and R). To each of these corresponds one of the DKT elements at the thin plate limit as indicated in the same figure.

Of particular interest is the last of the elements in which a very unorthodox formulation is used for the interpolation of θ and w variables. Here the interpolation of T is *incompatible*, i.e., not

automatically satisfying C^0 - continuity as apparently required by the functional of (22). (We note in passing that this continuity is *not* needed for w, and indeed the element of [3], Fig. 2b, does not impose this). However, the element still passes the general patch test [33] and is extensively used for thin plates. We believe it can similarly be used in thick plate situations.

9. Numerical results

A series of numerical tests have been conducted in order to assess the performance of the new triangles. In the results reported below, the 6-node elements are labeled TRI-6 and TRI-6R as discussed in Section 7.1. The 3-node element with a mid-side rotation described in Section 7.2 is labeled DRM (it is a discrete Reissner-Mindlin element equivalent to the DKT triangle presented in [8]). Each element imposes discrete shear constraints according to the Reissner-Mindlin theory. The elements have been incorporated into the Finite Element Analysis Program (FEAP) [40] and all computations have been conducted on a Micro VAX-II using double precision arithmetic and the F77 compiler in an Ultrix operating environment. The results are compared to exact solutions (or other approximate series or finite difference solutions) as well as to results obtained from some other finite elements. Tables are included to facilitate the comparisons.

9.1 Uniform loading on square plate

A quadrant of a square plate is modeled with different meshes and our triangular elements for simply supported boundary conditions. Both soft ($w = 0$) and hard ($w = 0$ and $\theta_s = 0$) boundary conditions are considered for the simply supported case. A typical mesh is shown in Fig. 10, mesh type A. The loading, consistent with the formulation, is given by equal vertical forces at each node. The results are reported in Table 1A and compared to an analytical solution (in a series form) for the thin plate limit [35]. For hard simply supported boundaries a correction to account for the shear deformation may be easily computed and added to the thin plate solution. A solution for the soft boundary is more complicated as the twist moments must be computed at each edge and set to zero.

Table 1A. Comparison of Elements - Thin Square Plate

	Simply Supported - Center Displacement - t/a = 1/100 ($\times 10^{-4}$)						Energy ($\times 10^{-5}$)
	Hard			Soft			
Mesh	Tri-6	Tri-6R	DRM	Tri-6	Tri-6R	DRM	DRM
2x2	4.4840	4.2179	4.0582	4.5943	4.2216	4.0903	4.0291
4x4	4.1873	4.1042	4.0671	4.2088	4.1100	4.0737	4.2030
8x8	4.0976	4.0749	4.0659	4.1088	4.0838	4.0719	4.2506
16x16	4.0731	4.0672	4.0649	4.0888	4.0823	4.0756	4.2676
Series (Thin)	4.0623	4.0623	4.0623	4.0623	4.0623	4.0623	
Series (Thick)	4.0644	4.0644	4.0644				

The structural properties of the plate for the results shown in Table 1A are

$$E = 10.92 \quad , \quad \nu = 0.3 \, ,$$

the side length is 10, the thickness is 0.1 and the uniform loading intensity, q, is 1.0.

The results given in Table 1A indicate that each of the element formulations is converging to the correct result. The DRM and TRI-6R generally provide superior results for all the cases considered. It should be noted that consideration of the center displacement is not sufficient to judge the results. While the center displacement may not always converge monotonically the total energy of the plate does (see Table 1A where results for the energy are included for a DRM problem).

The above problem is considered for the case where the thickness is increased to 1.0. This corresponds to a situation in which shear deformation is important. The results are presented in Table 1B for the center displacement. Again the results of the TRI-6R and DRM are superior to those for the TRI-6; however the results for all cases are converging. It should be noted that significant differences result from use of the two types of simply supported boundary conditions.

A quadrant of a square plate now is modeled with different meshes and the DRM element using simply supported and clamped boundary conditions. Both soft and hard boundary conditions are considered for the simply supported case. Two orientations (labeled A and B, see Fig. 10) are examined to indicate the sensitivity to different meshes. The results are reported in Table 1C and compared to an analytical solution (in a series form) for the thin plate limit from [35], and for the hard simply supported condition to the result with the shear correction. The data for the problem is

Table 1B. Comparison of Elements - Thick Square Plate

Uniform Loading - Center Displacement - t/a = 1/10						
	Simply Supported (x 10^{-1})					
	Hard			Soft		
Mesh	Tri-6	Tri-6	DRM	Tri-6	Tri-6	DRM
2x2	4.6950	4.4333	4.8665	4.9920	4.6329	4.3992
4x4	4.3961	4.3153	4.2829	4.6705	4.5684	4.4600
8x8	4.3061	4.2840	4.2739	4.6184	4.5900	4.5393
16x16	4.2818	4.2757	4.2728	4.6159	4.6082	4.5906
Series (Thick)	4.2728	4.2728	4.2728			

the same as above except the thickness is now set to 0.01 to represent a very thin case. The shear correction is now very small and the results are converging to the thin plate limit as expected. For comparison the solution for the DKT triangle is included for the hard boundary condition case and results are fully consistent with the DRM element. This further corroborates the statements included in section 8 concerning the use of discrete shear resultant constraints.

Table 1C. Simply Supported and Clamped Square Plate - DRM Element

Uniform Loading - Center Displacement (x 10^7) - t/a = 1/1000							
	Simply Supported					Clamped	
	Soft		Hard				
Mesh	A	B	A	B	DKT A	A	B
1x1	4.2811	2.3386	4.1615	2.3386	4.1615	1.8921	1.0365
2x2	4.0870	3.6839	4.0559	3.6756	4.0559	1.5474	1.2145
4x4	4.0689	3.9748	4.0649	3.9726	4.0649	1.3474	1.2578
8x8	4.0643	4.0410	4.0637	4.0406	4.0637	1.2866	1.2636
16x16	4.0630	4.0572	4.0628	4.0570	4.0628	1.2707	1.2649
Series -Thin[35]	4.0623	4.0623	4.0623	4.0623	4.0623	1.26	1.26
Series -Thick			4.0623	4.0623	4.0623		

For the hard boundary conditions the energy stored in the plate may also be computed from the series solutions including shear deformation. The results for the DRM element and mesh type A are given in Table 1D. These results may also be used to establish the rate of convergence in energy for the DRM element. The results reported here are computed from

$$U = \int_{\Omega} q(x,y)\, w(x,y)\, d\Omega$$

and, thus, are actually twice the strain energy (results in [4] appear to also be computed in this way).

Based upon this analysis the slope of the $\ln(U_{ex} - U_{\epsilon})$ vs. $\ln(h)$ is slightly greater than 2.

Table 1D. Uniform Load on Simply Supported Square Plate - Strain Energy

DRM - Hard Simply Supported Plate, Uniform Loading		
	Thickness	
	0.1	1.0
	Strain Energy in a Quadrant	
Mesh	$\times 10^{-5}$	$\times 10^{-2}$
1x1	3.469912	3.669961
2x2	3.997377	4.225539
4x4	4.195232	4.438442
8x8	4.243562	4.490909
16x16	4.255115	4.503337
32x32	4.257901	4.506331
Series-Thick	4.258787	4.507305
Series-Thin	4.256276	4.256276

In a recent paper by Babuska and Scapolla [4], a value for the strain energy in plates subjected to uniform loading has been determined using three dimensional elasticity solutions and a formulation similar to the Reissner-Mindlin plate theory. Their solutions may also be used to assess convergence properties of the triangular elements presented in this paper. The plate properties are given by modulus of elasticity, $E = 30. \times 10^6$, Poisson ratio,$\nu = 0.3$, side length a = 1, plate thickness t = 0.01 uniform loading q = 1.0 and shear shape factor $\kappa = 1$. In Table 1E we give the values of the strain energy for various mesh type A refinements using the three elements described in this paper. We also include the number of degrees-of-freedom which need to be solved in each formulation. This gives some insight to cost estimates for the alternative formulations.

The results from Table 1E indicate that our elements are converging to an energy which is slightly smaller than the one given in reference 4, which is stated to be slightly more accurate than a Reissner-Mindlin plate result.

9.2 Concentrated load on a square plate

The same tests on the DRM element as considered in Section 9.1 for Table 1C are performed,

Table 1E. Uniform Load on Simply Supported (Hard) Square Plate - Strain Energy

Strain Energy ($\times 10^3$) - t/a = 1/100						
Mesh/ Quadrant	D.O.F. (active)	Tri-6	D.O.F. (active)	Tri-6R	D.O.F. (active)	Tri-DRM
2x2	56	0.705719	44	0.645214	32	0.586560
4x4	208	0.646008	160	0.628663	112	0.611825
8x8	800	0.627962	608	0.623484	416	0.618676
16x16	3136	0.623969	2368	0.622808	1600	0.621027
Plate [4]		0.625413		0.625413		0.625413
3-D [4]		0.625956		0.625956		0.625956

the only difference being that the loading is now concentrated on the mid-point of the plate ($P=1.0$) and the plate thickness is set to 0.1. The displacement at the center of the plate for each mesh is contained in Table 2.

Table 2. Point Loading on Square Plate

Point Loading - Center Displacement (x 10^3) - t/a = 1/100						
	Simply supported				Clamped	
	Soft		Hard			
Mesh	A	B	A	B	A	B
1x1	1.2493	1.4039	1.2492	1.4039	0.5676	0.6226
2x2	1.1703	1.2852	1.1700	1.2850	0.5867	0.6371
4x4	1.1656	1.2019	1.1649	1.2014	0.5723	0.5926
8x8	1.1645	1.1750	1.1632	1.1738	0.5660	0.5726
16x16	1.1650	1.1678	1.1627	1.1656	0.5643	0.5663
Series solution	1.1600	1.1600	1.1600	1.1600	0.560	0.560

This is a problem for which the exact solution (according to the Reissner-Mindlin theory) under the point load is infinite. The solution for the thin plate limit is finite and is the one reported above. What is demonstrated by the problem is that the elements all tend to the limiting solution for the meshes used. We have, however, observed divergence from the limit (to larger solutions) for fine meshes and slightly thicker plates. Thus, it appears that if the mesh is refined about the point load our results do indeed become larger than the thin plate results and begin to exhibit the nature of the displacement singularity predicted by the Reissner-Mindlin theory.

9.3 Circular plate under uniform loading

Due to symmetry, one quadrant of a circular plate has been discretized with five different meshes. The mesh shown in Fig. 11 is for the 96 element model. Results for clamped and simply supported boundary conditions are computed for a thick (R/t = 5/1) and a relatively thin (R/t = 5/0.1) plate. Two types of simply supported boundary conditions are considered. The first is the soft condition used for the square plate problems and is imposed by setting only the displacements $\bar{w}$ zero at each boundary node. The second form transforms the rotation parameters to tangential and normal components and restrains only the tangential component together with the transverse displacement at each node. Each $\Delta\theta^k$ is also restrained on a boundary segment. This defines a hard simply supported condition and is consistent with results for the thin plate limit. It should be noted in Table 3a that the results for the two different boundary conditions give the same limit solution for the thick plate problem. This is consistent with the one dimensional character of the solution in which θ_t and M_{nt} vanish simultaneously when w is set to zero. The results are compared in Table 3a with the analytical solution which gives a center displacement for the clamped boundary of

$$w(0) = \frac{q\,a^4}{64D}\left[1 + \frac{8}{3\kappa(1-\nu)}\left(\frac{t}{a}\right)^2\right]$$

and for the simply supported case

$$w(0) = \frac{q\,a^4}{64D}\left[\frac{5+\nu}{1+\nu} + \frac{8}{3\kappa(1-\nu)}\left(\frac{t}{a}\right)^2\right]$$

Exact energy expressions may be computed for this problem and are given by

$$E_{CL} = \frac{q^2 a^6 \phi}{384D}\left[1 + \frac{4}{\kappa(1-\nu)}\left(\frac{t}{a}\right)^2\right]$$

for the clamped case (where ϕ defines the size of the sector analyzed - $\frac{\pi}{2}$ for our analyses) and

$$E_{SS} = \frac{q^2 a^6 \phi}{384D}\left[\frac{7+\nu}{1+\nu} + \frac{4}{\kappa(1-\nu)}\left(\frac{t}{a}\right)^2\right]$$

for the simply supported case. It should be noted that the energy expressions represent the total work done by the external loads and thus are twice the internal strain energy in the plate. Results for our analyses are given in Table 3b.

Table 3a. Center Displacement for Simply Supported and Clamped Circular Plate under Uniform Loading (R = 5)

	Plate Thickness					
	t = 0.1			t = 1.0		
Mesh	Clamp	Soft	Hard	Clamp	Soft	Hard
6-element	10315.6	37857.7	37857.7	11.9924	39.6043	39.6043
24-element	9999.91	39401.5	39373.8	11.7775	41.2023	41.1514
96-element	9850.93	39732.1	39727.5	11.6305	41.5172	41.5069
384-element	9802.40	39808.2	39807.4	11.5745	41.5810	41.5795
1536-element	9788.74	39826.2	39826.0	11.5577	41.5952	41.5950
Exact solution	9783.48	39831.5	39831.5	11.55	41.60	41.60

The material properties of the plate are

$$E = 10.92 \quad , \quad \nu = 0.3 \, ,$$

which gives a plate stiffness, D, of t^3, and the uniform loading q is 1.0

Table 3b. Energy for Simply Supported and Clamped Circular Plate under Uniform Loading (R = 5)

	Plate Thickness			
	t = 0.1		t = 1.0	
Mesh	Clamp	SS	Clamp	SS
6-element	67761.576	290946.555	80.998467	304.775672
24-element	66320.253	341303.887	82.781478	358.088806
96-element	64804.242	354622.658	82.023468	371.930150
384-element	64295.393	357984.088	81.624299	375.325303
1536-element	64150.286	358818.561	81.495286	376.164563
Exact solution	64091.178	359087.484	81.447075	376.443338

9.4 Skew plate with two opposite edges simply supported others free [41]

This is a 60° skew plate, simply supported on two opposite sides and free on the other two (see Fig. 12). It is subjected to uniform loading and the transverse displacement of the middle point is reported. Figure 12 also compares the accuracy of the solution to the one obtained in [41], as a function of the number of degrees of freedom involved in each case.

Table 4. Skew plate as in [41]

Mesh	b.c.	w (x $10^2 qL^4/D$)	M_y (x $10^1 qL^2$)
2x2	Soft	0.6338	0.6297
	Hard	0.6392	0.6262
4x4	Soft	0.7558	0.8886
	Hard	0.7527	0.8870
6x6	Soft	0.7766	0.9287
	Hard	0.7742	0.9272
8x8	Soft	0.7822	0.9424
	Hard	0.7838	0.9418
12x12	Soft	0.7881	0.9523
	Hard	0.7891	0.9519
16x16	Soft	0.7909	0.9557
	Hard	0.7903	0.9554
32x32	Soft	0.7927	0.9589
	Hard	0.7925	0.9588
Series		0.7945	0.9589

All the properties and geometric data for this problem are given in [41].

9.5 Skew cantilever plate [8]

A rhombic cantilever plate with a skew of 45° and subjected to uniform loading is tested in [8] for the thin limit and the results obtained using a DKT and an HSM element [11] are reported and compared with experimental values. The same analysis is repeated using the new DRM triangle and all the results are compared in Table 5.

Table 5. Skew cantilever plate [8]

	Deflection at location					
	1	2	3	4	5	6
DRM	0.304	0.199	0.113	0.121	0.056	0.023
DKT	0.304	0.198	0.113	0.121	0.056	0.023
HSM	0.264	0.173	0.100	0.095	0.043	0.021
Experimental value	0.297	0.204	0.121	0.129	0.056	0.022

Again, all the plate parameters are specified in [8].

9.6 Simply supported skew plate

A skew plate which is simply supported on all edges is analyzed for the case of uniform loading. A typical mesh is illustrated in Fig. 13. The skew angle results in interior vertex angles of 30^o and 150^o. For this angle a moment singularity results at each 150^o vertex. The simply supported edges are treated as soft and results are tabulated in Table 6A for the center displacement of a plate with thickness 1.0; and in Table 6B we consider the more difficult problem of a plate with a thickness of 0.1. The results obtained for a set of meshes are compared with those of other elements and with a solution given in [24] for the "thin" plate.

Table 6A. Uniform Load on 30^o Simply Supported (Soft) Rhombic Plate

Center Displacement - t/a = 1/100					
Side Nodes[9]	Tri-6	Tri-6R	Tri-DRM	T1 [19]	Simo *et. al.* [31]
3	0.09920	0.04859	0.06844	0.00279	-
5	0.07075	0.05739	0.04955	0.03918	0.04282
9	0.05655	0.04161	0.04646	0.03899	0.04264
17	0.04875	0.04299	0.04601	0.04187	0.04387
33	0.04675	0.04491	0.04590	0.04410	0.04496
Ref [23]	0.04455	0.04455	0.04455	0.04455	0.04455

The plate properties are given by

$$E = 10. \times 10^6 \ ; \ \nu = 0.3 \ ;$$

Side length a = 100, plate thickness t = 1.0 (for Table 6A) and 0.1 (for Table 6B) and uniform loading q = 1.0

The comparison solution recently computed by Babuska and Scapolla [4] provides a value for the strain energy which may also be used to assess convergence properties of the element. As before, their plate properties are given by

$$E = 30. \times 10^6 \ ; \ \nu = 0.3 \ ;$$

Side length a = 1, plate thickness t = 0.01 uniform loading q = 1.0 and shear shape factor $\kappa = 1$.

[9] The Tri-6 elements are treated as quadratic with the mid-side unknowns counted as a node. The DRM element counts only vertex nodes.

Table 6B. Uniform Load on 30° Thin Simply Supported (Soft) Rhombic Plate

Center Displacement - t/a = 1/1000			
Side Nodes	Tri-6	Tri-6R	Tri-DRM
3	99.11	48.47	68.34
5	70.51	57.19	49.44
9	55.39	39.78	46.32
17	45.60	37.83	45.79
33	43.25	39.28	45.49
Ref [23]	44.55	44.55	44.55

In Table 6C we give the values of the strain energy for various mesh refinements using the elements described in this paper.

Table 6C. Uniform Load on a 30° Simply Supported (Soft) Rhombic Plate - Strain Energy

Strain Energy ($\times 10^4$) - t/a = 1/100						
Mesh Elements	D.O.F. (active)	Tri-6	D.O.F. (active)	Tri-6R	D.O.F. (active)	Tri-DRM
1x1	19	0.551028	14	0.269828	-	-
2x2	59	0.408832	43	0.284542	35	0.285103
4x4	211	0.336567	155	0.246947	115	0.256943
8x8	803	0.286247	595	0.250380	419	0.261289
16x16	3139	0.269838	2339	0.258260	1603	0.262455
32x32	-	-	-	-	6275	0.262708
Plate Ref [4]		0.265509		0.265509		0.265509
3-D Ref [4]		0.265868		0.265868		0.265868

Again, our results generally are converging to a result slightly smaller than those given in reference 4. The results of the skew plate analyses tend to favor the overall superiority of the DRM element to solve a wide class of problems. The other problems considered do not give significantly different answers for the DRM and the TRI-6R elements. The TRI-6 element is quite flexible in most of the analyses conducted. The DRM element has significantly fewer degrees-of-freedom in each problem (approximately two-thirds the number in the TRI-6R formulation and half the number in TRI-6) thus the element provides excellent results at the least cost of all the elements considered in this paper.

9.7 Sensitivity test

A test on the influence of element distortion in modeling a clamped plate has been performed using the DRM element on a relatively crude mesh of 8 triangles. The plate has a side length of 12 (6 units for one quadrant) and the center node is moved as far as the quarter points of the quadrant, Fig. 14. The results reported in Table 7 show that the element displays insignificant sensitivity when the geometry is altered within these limits. This is, obviously, a highly desired feature for any element.

Table 7. Sensitivity test on a clamped, uniformly loaded plate

Center Displacement (x 10^{-3})		
(x,y) - Coordinates of Interior Node	w	% error (relative)
(3.00,3.00)	3.35729	0.00
(3.25,3.25)	3.35462	0.08
(3.50,3.50)	3.34660	0.31
(3.75,3.75)	3.33313	0.72
(4.00,4.00)	3.31356	1.30
(4.25,4.25)	3.28403	2.18
(3.00,3.25)	3.35548	0.05
(3.00,3.50)	3.35318	0.12
(3.00,3.75)	3.35025	0.21
(3.00,4.00)	3.34640	0.32
(3.00,4.25)	3.34123	0.48
(3.00,4.50)	3.33431	0.68
(2.75,3.25)	3.35606	0.04
(2.50,3.50)	3.35991	0.08
(2.25,3.75)	3.37107	0.41
(2.00,4.00)	3.39206	1.04
(1.75,4.25)	3.42524	2.02
(1.50,4.50)	3.47146	3.40

10. Concluding remarks

This paper has presented a method for constructing mixed finite element approximations based upon the Reissner-Mindlin plate bending theory. The mixed approximation involves specification of the transverse displacement, w, the rotations, θ, and the shearing resultants, S, (or alternatively, shearing strains γ). Discrete constraints are used to express the parameters in the shearing resultants in terms of displacement parameters; hence, the formulation presented may be directly used in

standard finite element packages. By suitable choice of constraints the elements generated pass the mixed patch test and, thus, do not lock and are not singular in the thin plate limit. The methodology presented also provides a unification with previous developments which used discrete Kirchhoff constraints.

New triangular elements are presented and shown to give good results on a series of standard test problems. For the limiting case of thin plate behavior, the DRM element (for discrete Reissner-Mindlin element) is shown to be identical to the popular DKT triangle introduced by Dhatt [13]. Unlike the DKT element, however, the DRM element also may be used for analysis of "thick" plate problems.

Since interpolation is provided for all the variables in the formulation the extension to transient, as well as non-linear applications is straight forward. Furthermore, we believe that the DRM element presented is suitable for use with adaptive mesh refinement schemes.

References

1. S. Ahmad, B. M. Irons and O. C. Zienkiewicz, "Curved thick shell and membrane elements with particular reference to axisymmetric problems," *Proc. 2nd Conf. on Matrix Methods in Structural Mechanics,* Wright-Patterson Air Force Base, Ohio, 1968.
2. S. Ahmad, B. M. Irons and O. C. Zienkiewicz, "Analysis of thick and thin shell structures by curved finite elements," *Int. J. Numer. Meth. Eng.*, **2,** 419-451, 1970.
3. D. N. Arnold and R. S. Falk, "A uniformly accurate finite element method for Mindlin-Reissner plate," *IMA Preprint Series No. 307,* Institute for Mathematics and its Applications, University of Minnesota, April 1987.
4. I. Babuska and T. Scapolla, "Benchmark computation and performance evaluation for a rhombic plate bending problem," *Int. J. Numer. Meth. Eng.*, **27,** 155-179, 1989.
5. J. T. Baldwin, A. Razzaque and B. M. Irons, "Shape function subroutine for an isoparametric thin plate element," *Int. J. Numer. Meth. Eng.*, **7,** 431-xxx, 1972.
6. K. J. Bathe and E. N. Dvorkin, "A four node plate bending element based on Mindlin/Reissner plate theory and mixed interpolation," *Int. J. Numer. Meth. Eng.*, **21,** 367-383, 1985.
7. J. L. Batoz, "An explicit formulation for an efficient triangular plate bending element," *Int. J. Numer. Meth. Eng.*, **18,** 1077-1089, 1982.
8. J. L. Batoz, K. J. Bathe and L. W. Ho, A study of three node triangular plate bending elements," *Int. J. Numer. Meth. Eng.*, **15,** 1771-1812, 1980.
9. J. L. Batoz and M. Ben Tohar, "Evaluation of a new quadrilateral thin plate bending element," *Int. J. Numer. Meth. Eng.*, **18,** 1655-1677, 1982.
10. K. J. Bathe, E. N. Dvorkin and L. W. Ho, "On discrete Kirchhoff and isoparametric shell elements for nonlinear analysis - an assessment," *J. Comp. Struct.*, **16,** 89-98, 1982.
11. R. W. Clough and J. L. Tocher, "Finite element stiffness matrices for analysis of plates in bending," *Proc. Conf. on Matrix Meth. in Struct. Mech.*, **AFFDL-TR-66-80,** WPAFB, Ohio, 515-545, 1966.
12. M. A. Crisfield, "A four-noded thin-plate bending element using shear constrains - a modified version of Lyon's element," Comp. Meth. Appl. Mech. Eng., **38,** 93-120, 1983.
13. G. S. Dhatt, "Numerical analysis of thin shells by curved triangular elements based on discrete Kirchhoff hypothesis," *Proc. Symp Appl. of F.E.M. in Civil Eng. (W. R. Rowan and R. M. Hackett, eds.),* Vanderbilt University, Nashville, Tennessee, 1969.
14. E. N. Dvorkin and K. J. Bathe, "A continuum mechanics based four node shell element for general non-linear analysis," *Eng. Comp.*, **1,** 77-88, 1984.
15. E. Hinton and H. C. Huang, "A family of quadrilateral Mindlin plate elements with substitute shear strain fields," *Comp. and Struct.*, **23,** 409-431, 1986.
16. H. C. Huang and E. Hinton, "A nine node Lagrangian Mindlin element with enhanced shear interpolation," *Eng. Comp.*, **1,** 369-380, 1984.
17. T. J. R. Hughes, **The Finite Element Method,** Prentice-Hall, Englewood Cliffs, N.J., 1987.
18. T. J. R. Hughes, R. L. Taylor and W. Kanoknukulchai, "A simple and efficient element for plate bending," Int. J. Numer. Meth. Eng., **11,** 1529-1543, 1977.
19. T. J. R. Hughes and T. E. Tezduyar, "Finite elements based upon Mindlin plate theory with particular reference to the four node bilinear isoparametric element," *J. Appl. Mech.*, **46,** 587-596, 1981.
20. L. P. R. Lyons, "A general finite element system with special analysis of cellular structures," Doctoral dissertation, Imperial College of Science and Technology, London, 1977.

21. D. S. Malkus and T. J. R. Hughes, "Mixed finite element methods - reduced and selective integration techniques: A unification of concepts," *Comp. Meth. Appl. Mech. Eng.*, **15**, 63-81, 1978.

22. R. D. Mindlin, "Influence of rotatory inertia and shear in flexural motions of isotropic elastic plates," *J. Appl. Mech.*, **18**, 31-38, 1951.

23. L. S. D. Morley, **Skew Plates and Structures**, International Series of Monographs in Aeronautics and Astronautics, MacMillan, New York, 1963.

24. S. S. Murthy and R. H. Gallagher, "A triangular thin-shell finite element based on discrete Kirchhoff theory," *Comp. Meth. Appl. Mech. Eng.*, **54**, 197-222, 1986.

25. J. C. Nagtegaal and S. Nakazawa, "On the construction of optimal Mindlin type plate and shell elements," **Finite Element Methods for Plate and Shell Structures**, Volume 1: Element Technology, (T. J. R. Hughes and E. Hinton, eds.), Pineridge Press, 1986.

26. S. F. Pawsey and R. W. Clough, "Improved numerical integration of thick slab finite elements," *Int. J. Numer. Meth. Eng.*, **3**, 575-586, 1971.

27. E. D. L. Pugh, E. Hinton and O. C. Zienkiewicz, "A study of quadrilateral plate bending elements with reduced integration," *Int. J. Numer. Meth. Eng.*, **12**, 1059-1079, 1978.

28. A. Razzaque, "Finite element analysis of plates and shells," Doctoral dissertation, Civil Engineering, University College of Swansea, 1972.

29. A. Razzaque, "Program for triangular bending elements with derivative smoothing," *Int. J. Numer. Meth. Eng.*, **6**, 333-345, 1973.

30. E. Reissner, "The effect of transverse shear deformation on the bending of elastic plates," *J. Appl. Mech.*, **12**, 69-76, 1945.

31. J. C. Simo, D. D. Fox and M. S. Rifai, "On a stress resultant geometrically exact shell model. Part II: The linear theory; computational aspects," *Comp. Meth. Appl. Mech. Eng.*, (to appear 1989).

32. H. Stolarski and M. Y. M. Chiang, "Thin plate elements with relaxed Kirchhoff constraints," *Int. J. Numer. Meth. Eng.*, **26**, 913-934, 1988.

33. R. L. Taylor, O. C. Zienkiewicz, J. C. Simo, and A. H. C. Chan, "The patch test - a condition for assessing FEM convergence," *Int. J. Numer. Meth. Eng.*, **22**, 32-62, 1986.

34. A. Tessler and S. B. Dong, "On a hierarchy of conforming Timoshenko beam elements," *Comp. and Struct.*, **14** 335-344, 1981.

35. S. Timoshenko and S. Woinowsky-Krieger, **Theory of Plates and Shells** McGraw Hill, New York, 1959.

36. G. A. Wempner, J. T. Oden, and D. K. Dross, "Finite element analysis of thin shells," *Proc. Am. Soc. Civ. Eng*, **EM6**, 1273-94, 1968.

37. K. Washizu, **Variational Methods in Elasticity and Plasticity**, Pergamon Press, Oxford, 1948.

38. F.-G. Yuan and R. E. Miller, "A cubic triangular finite element for flat plates with shear," *Int. J. Numer. Meth. Eng.*, **28**, 109-126, 1989.

39. O. C. Zienkiewicz, **The Finite Element Method**, 3rd Edition, McGraw Hill, London, 1977.

40. O. C. Zienkiewicz and D. Lefebvre, "Three field mixed approximation and the plate bending problem," *Comm. Appl. Numer. Meth.*, **3**, 301-309, 1987.

41. O. C. Zienkiewicz and D. Lefebvre, "A robust triangular plate bending element of the Reissner-Mindlin type," *Int. J. Numer. Meth. Eng.*, **26**, 1169-1184, 1988.

42. O. C. Zienkiewicz, J. Too and R. L. Taylor, "Reduced integration technique in general analysis of plates and shells," *Int. J. Numer. Meth. Eng.*, **3**, 275-290, 1971.

43. O. C. Zienkiewicz, S. Qu, R. L. Taylor and S. Nakazawa, "The patch test for mixed formulations," *Int. J. Numer. Meth. Eng.*, **23**, 1873-1883, 1986.

APPENDIX A - Transverse Shear Resultant Interpolation

The interpolation described in section 7 for the transverse shear resultant is given by

$$\mathbf{S} = \sum_{i=1}^{3} L_i \bar{\mathbf{S}}^i \tag{A1}$$

The $\bar{\mathbf{S}}^i$ are to be determined by satisfying discrete edge constraints for the tangential shear resultant [33]. The tangential shear resultant on side k of the triangle (i.e., the side where $L_k = 0$) is

$$S_k = \mathbf{e}_k \cdot \mathbf{S} \tag{A2}$$

where

$$\mathbf{e}_k = [e_{kx}, e_{ky}] = [\cos\omega_k, \sin\omega_k] \tag{A3}$$

and ω_k is the angle that the tangent makes with the x–axis (see Appendix B).

Equation (A2) is used at two points on each side of the triangle to define 6 independent values of tangential shear resultant. The two points on each edge are picked to correspond to the two-point Gauss values, which on the interval 0 to 1 (range of each area coordinate) are given by

$$p_1 = \frac{1}{2}\left(1 + \frac{1}{\sqrt{3}}\right) \quad , \quad p_2 = \frac{1}{2}\left(1 - \frac{1}{\sqrt{3}}\right) \tag{A4}$$

Accordingly

$$\bar{S}_{k1} = S_k(L_{i1}, L_{j1}, L_{k1}) = \mathbf{e}_k \cdot \mathbf{S}(L_{i1}, L_{j1}, L_{k1}) \tag{A5a}$$

where

$$L_{i1} = p_1 \quad , \quad L_{j1} = p_2 \quad , \quad L_{k1} = 0$$

Similarly for the second point

$$\bar{S}_{k2} = S_k(L_{i2}, L_{j2}, L_{k2}) = \mathbf{S}(L_{i2}, L_{j2}, L_{k2}) \cdot \mathbf{e}_k \tag{A5b}$$

with

$$L_{i2} = p_2 \quad , \quad L_{j2} = p_1 \quad , \quad L_{k2} = 0$$

In the above the i, j, k sequence is given by (see Fig. 6) $j = mod(i, 3) + 1$, $k = mod(j, 3) + 1$.

Evaluation of (A5a,b) on each edge using (A1) gives

$$\bar{S}_{k1} = \mathbf{e}_k \cdot (p_1 \bar{\mathbf{S}}^i + p_2 \bar{\mathbf{S}}^j) \tag{A6a}$$

Similarly for the second point

$$\bar{S}_{k2} = \mathbf{e}_k \cdot (p_2 \bar{\mathbf{S}}^i + p_1 \bar{\mathbf{S}}^j) \tag{A6b}$$

Adding and subtracting (A6a) and (A6b) and simplifying the results we obtain

$$\mathbf{e}_k \cdot \bar{\mathbf{S}}^i = g_1 \bar{S}_{k1} + g_2 \bar{S}_{k2} \tag{A7a}$$

and

$$\mathbf{e}_k \cdot \bar{\mathbf{S}}^j = g_2 \bar{S}_{k1} + g_1 \bar{S}_{k2} \tag{A7b}$$

where

$$g_1 = \frac{1}{2}(1+\sqrt{3}) \quad , \quad g_2 = \frac{1}{2}(1-\sqrt{3}) \tag{A8}$$

The parameters $\bar{\mathbf{S}}^i$ now may be expressed in terms of the $\bar{S}_{i1}$ and $\bar{S}_{i2}$ using (A7a) directly, permuting the subscripts on (A7b) to correspond to the i value, and writing the pair of equations

$$\begin{Bmatrix} \mathbf{e}_k \cdot \bar{\mathbf{S}}^i \\ \mathbf{e}_j \cdot \bar{\mathbf{S}}^i \end{Bmatrix} = \begin{Bmatrix} g_1 \bar{S}_{k1} + g_2 \bar{S}_{k2} \\ g_2 \bar{S}_{j1} + g_1 \bar{S}_{j2} \end{Bmatrix} \tag{A9}$$

Upon noting that

$$\begin{Bmatrix} \mathbf{e}_k \cdot \bar{\mathbf{S}}^i \\ \mathbf{e}_j \cdot \bar{\mathbf{S}}^i \end{Bmatrix} = \begin{bmatrix} e_{kx} & e_{ky} \\ e_{jx} & e_{jy} \end{bmatrix} \begin{Bmatrix} \bar{S}_x^i \\ \bar{S}_y^i \end{Bmatrix} \tag{A10}$$

the solution is given by

$$\begin{Bmatrix} \bar{S}_x^i \\ \bar{S}_y^i \end{Bmatrix} = \frac{1}{\Delta_i} \begin{bmatrix} e_{jy} & -e_{ky} \\ -e_{jx} & e_{kx} \end{bmatrix} \begin{Bmatrix} g_1 \bar{S}_{k1} + g_2 \bar{S}_{k2} \\ g_2 \bar{S}_{j1} + g_1 \bar{S}_{j2} \end{Bmatrix} \tag{A11}$$

where

$$\Delta_i = e_{kx} e_{jy} - e_{ky} e_{jx}$$

Substitution of (A11) into (A1) gives the result presented as equation (31) of Section 7.

For the case in which the tangential shear is to be constant on each edge we may note that setting

$$\bar{S}_{k0} = \bar{S}_{k1} = \bar{S}_{k2} \tag{A12}$$

results immediately in the results given in equation (32).

APPENDIX B - Constraint equations for $\bar{S}_{kn}$

The parameters $\bar{S}_{k1}$, etc., may be expressed in terms of the nodal values of the transverse displacement, $\bar{w}$, and the rotations, $\bar{\theta}$, using results in (24) specialized for the tangential direction. Accordingly,

$$\frac{1}{\alpha}\bar{S}_{k1} = \left(\frac{\partial w}{\partial t} + \theta_t\right)\Big|_1 \tag{B1a}$$

$$= \pm\frac{\bar{w}^j - \bar{w}^i + 4(3^{-\frac{1}{2}})\Delta\bar{w}^k}{h_k} + \frac{1}{2}\mathbf{e}_k\cdot[\bar{\boldsymbol{\theta}}^i + \bar{\boldsymbol{\theta}}^j + 3^{-\frac{1}{2}}(\bar{\boldsymbol{\theta}}^i - \bar{\boldsymbol{\theta}}^j)] + \frac{2}{3}\Delta\theta^k$$

Similarly, for the second point

$$\frac{1}{\alpha}\bar{S}_{k2} = \left(\frac{\partial w}{\partial t} + \theta_t\right)\Big|_2 \tag{B1b}$$

$$= \pm\frac{\bar{w}^j - \bar{w}^i - 4(3^{-\frac{1}{2}})\Delta\bar{w}^k}{h_k} + \frac{1}{2}\mathbf{e}_k\cdot[\bar{\boldsymbol{\theta}}^i + \bar{\boldsymbol{\theta}}^j - 3^{-\frac{1}{2}}(\bar{\boldsymbol{\theta}}^i - \bar{\boldsymbol{\theta}}^j)] + \frac{2}{3}\Delta\theta^k$$

where h_k is the length of the k-side of the element.

The parameter $\bar{S}_{k0}$ for the DRM element may be deduced using (24) in (19). After integration along each boundary the result is

$$\frac{1}{\alpha}\bar{S}_{k0} = \int_{\Gamma_k}\left(\frac{\partial w}{\partial t} + \theta_t\right)dt = \pm\frac{\bar{w}^j - \bar{w}^i}{h_k} + \frac{1}{2}\mathbf{e}_k\cdot(\bar{\boldsymbol{\theta}}^i + \bar{\boldsymbol{\theta}}^j) + \frac{2}{3}\Delta\theta^k \tag{B2}$$

The $\pm$ ambiguity in (B1) and (B2) is due to the fact that the direction of the tangential shear must be defined by a unique direction on each edge of contiguous elements. Failure to achieve this, results in an inconsistent definition of the edge incremental rotation degree-of-freedom, $\Delta\theta^k$. One way to overcome this difficulty is to define the direction for $\mathbf{e}_k$ in the direction of increasing (global) node numbers for the end points of each element edge, thus establishing a unique value for ω_k. The sign in (B1) and (B2) is chosen to be positive if the direction of $\mathbf{e}_k$ corresponds to that for constructing the boundary integrals, otherwise a negative sign is inserted.

The construction of $\mathbf{Q}_w$ and $\mathbf{Q}_\theta$ in (21b) is obtained by a systematic use of (B1) or (B2) and noting that the shape functions for shear are given by the area coordinates, L_i, as shown in equation (A1).

The result for a DKT element can be obtained by setting (B2) to zero and expressing each $\Delta\theta^k$ in terms of the nodal parameters at each vertex of the triangle. The resulting element has 9 degrees-of-freedom (3 at each node) and is identical to the results given in references 7, 8, and 13.

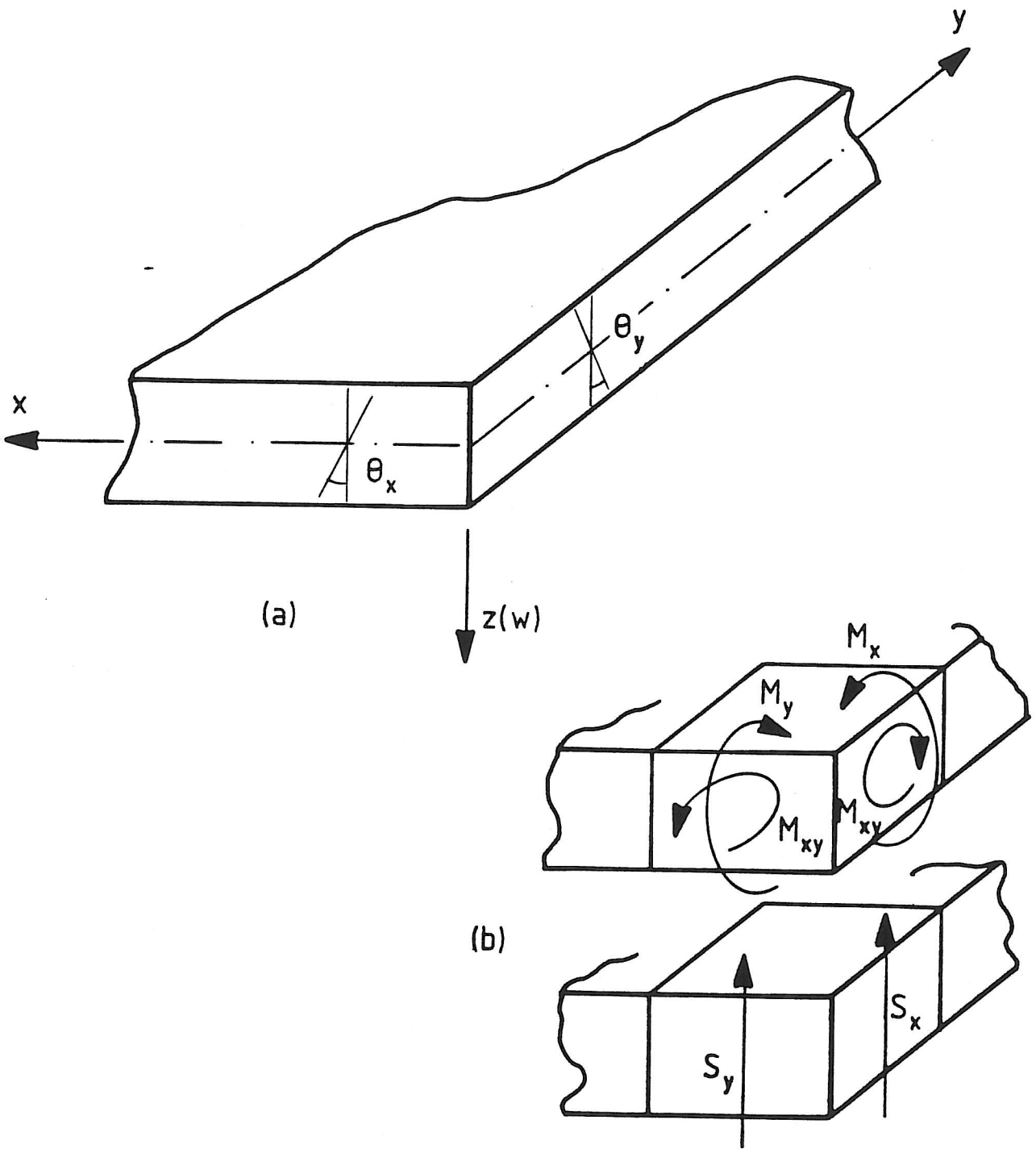

FIGURE 1 DEFINITIONS OF VARIABLES FOR PLATE EQUATIONS
(a) Displacements & rotations
(b) Stress resultants

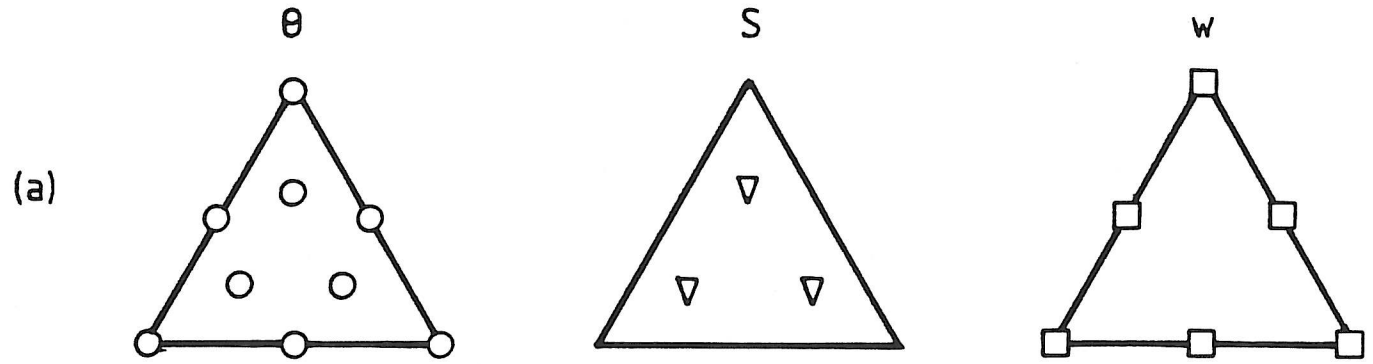

	n_θ	n_S	n_w	
TEST C	$n_\theta = 6$	$n_S = 6$	$n_w = 0$	(pass)
TEST R	$n_\theta = 18-2 = 16$	$n_S = 6$	$n_w = 6-1 = 5$	(pass.

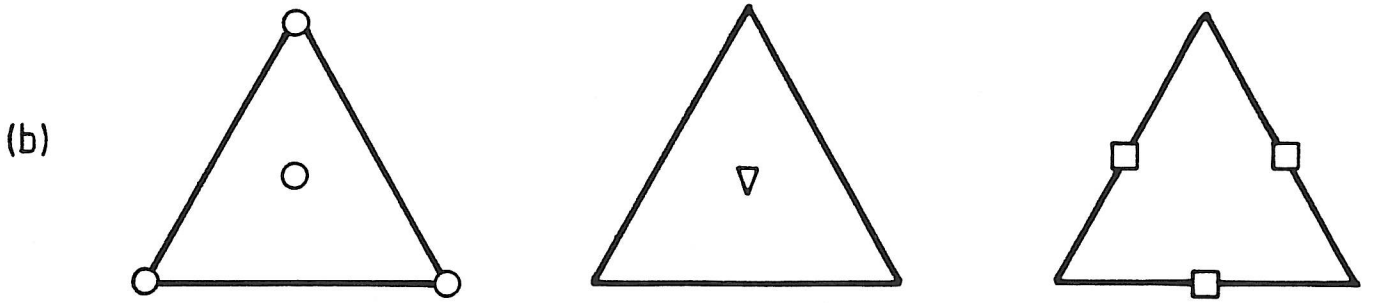

	n_θ	n_S	n_w	
TEST C	$n_\theta = 2$	$n_S = 2$	$n_w = 0$	(pass)
TEST R	$n_\theta = 8-2 = 6$	$n_S = 2$	$n_w = 3-1 = 2$	(pass)

FIGURE 2 SINGLE ELEMENT PATCH TEST COUNT
(a) Element of Ref 9 (Zienkiewicz-Lefebvre)
(b) Element Ref 28 (Arnold)

○ Node with $\underset{\sim}{\theta}$ variables (2 DOF)
▽ Node with $\underset{\sim}{S}$ variables (2 DOF)
□ Node with w variables (1 DOF)

(Constrained) TEST C All θ - w prescribed on boundary
(Relaxed) TEST R 2θ and 1w variables on boundary prescribed

Necessary condition : $n_\theta + n_w > n_s$
$n_s > n_w$

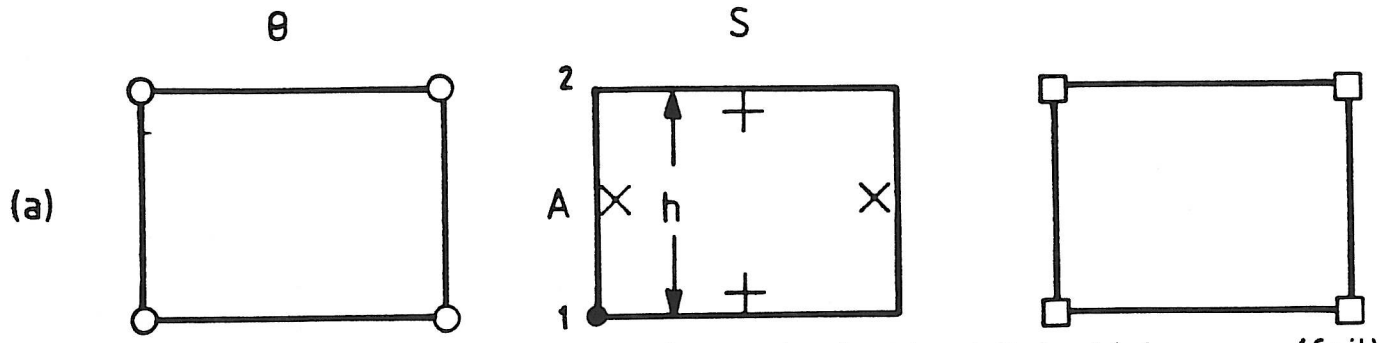

TEST C $n_\theta = 0$ $\left\{ \begin{array}{l} n_S = 4 \text{ standard Galerkin)} \\ n_S = 0 \text{ with collocation} \end{array} \right.$ (fail) $n_w = 0$ (pass)

TEST R $n_\theta = 8-2=6$ $n_S = 4$ $n_w = 4-1=3$ (pass)

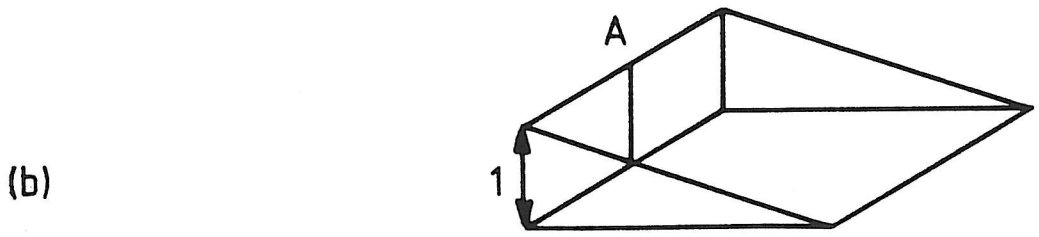

FIGURE 3 THE DVORKIN-BATHE ELEMENT

(a) The element parameters

- ○ θ nodes (2 DOF)
- \+ S_y nodes (1 DOF) } eliminated at element level
- × S_x nodes (1 DOF) }
- □ w nodes (1 DOF)

(b) Shape function for S_x at node A

Note : With collocation type of constraint along 1-2 S_y at A is determined value by θ/ω at (1) and (2) and hence not a full parameter This ensures that test is satisfied.

Identified in collocation

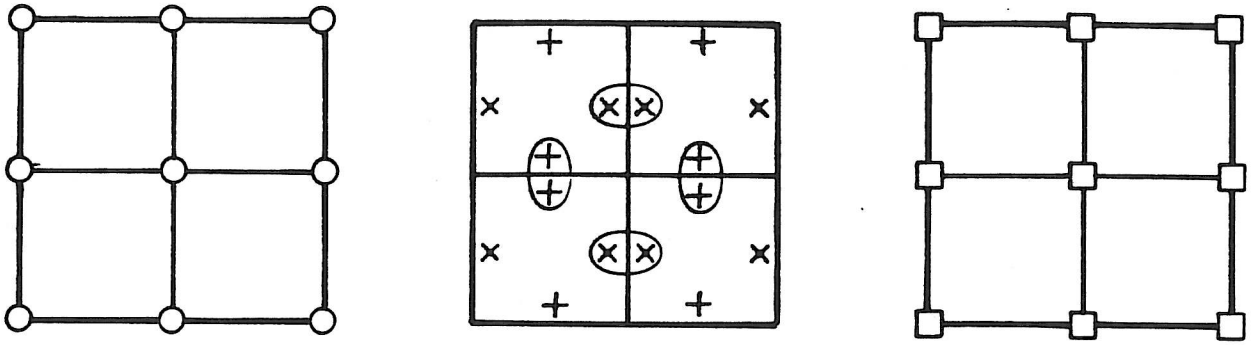

I STANDARD WEIGHTING

TEST C	$n_\theta = 2$	$n_S = 16$	$n_w = 1$	(fail)
TEST R	$n_\theta = 18-2 = 16$	$n_S = 16$	$n_w = 9-1 = 8$	(pass)

II BOUNDARY COLLOCATION

TEST C	$n_\theta = 2$	$n_S = 4$	$n_\omega = 1$	(fail)
TEST R	$n_\theta = 16$	$n_S = 12$	$n_\omega = 8$	(pass)

FIGURE 4 FOUR ELEMENT PATCH COUNT TEST ON QUADRIATERAL WITH S_x, S_y INTERPOLATION (DVORKIN-BATHE ELEMENT)
I STANDARD WEIGHTING
II COLLOCATION ON BOUNDARY

① Note : The Dvorkin-Bathe element fails this test , end is suspect in some circumstances (not robust)

② Note : With collocation S boundary values are prescribed by displacements on same line

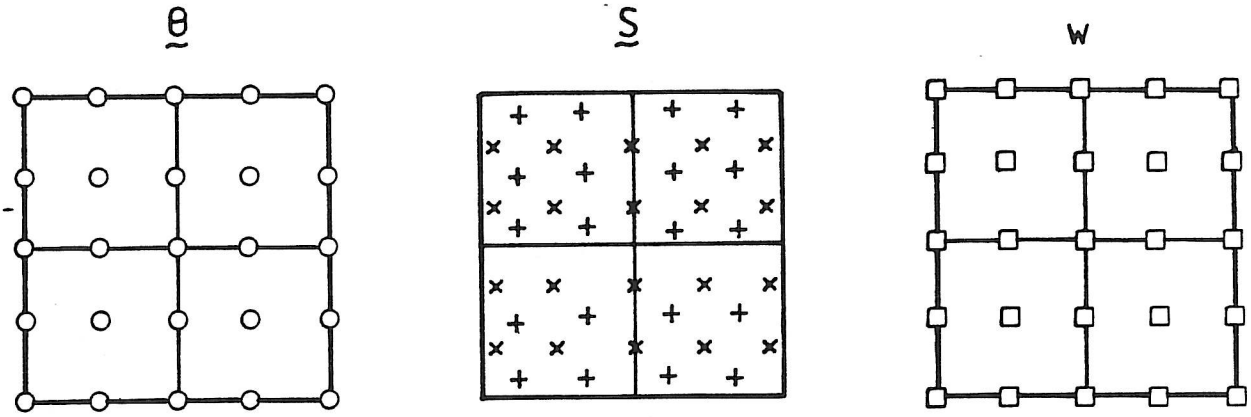

(a)

	$\underset{\sim}{\theta}$	$\underset{\sim}{S}$	w
Test C	$n_\theta = 18$	$n_S = 24$	$n_w = 9$
Test R	$n_\theta = 50-2 = 48$	$n_S = 40$	$n_w = 25-1 = 24$

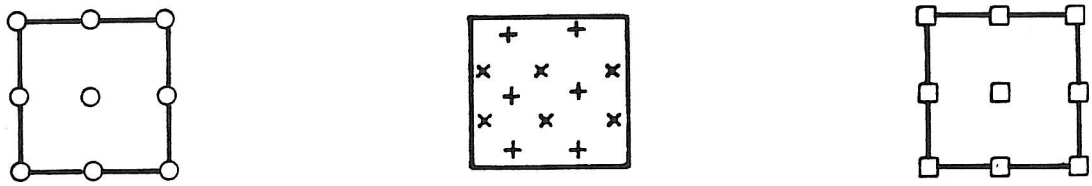

(b)

Test C	$n_\theta = 2$	$n_S = 4$	$n_w = 1$ (fail)
Test R	$n_\theta = 18-2 = 16$	$n_S = 12$	$n_w = 9-1 = 8$

FIGURE 5 FOUR ELEMENT (a) AND SINGLE ELEMENT (b) PATCH COUNT TEST ON THE HINTON-HUANG ELEMENT
(Two point boundary collocation only shown)

Note : This is a robust element as all multiple element patch tests passed

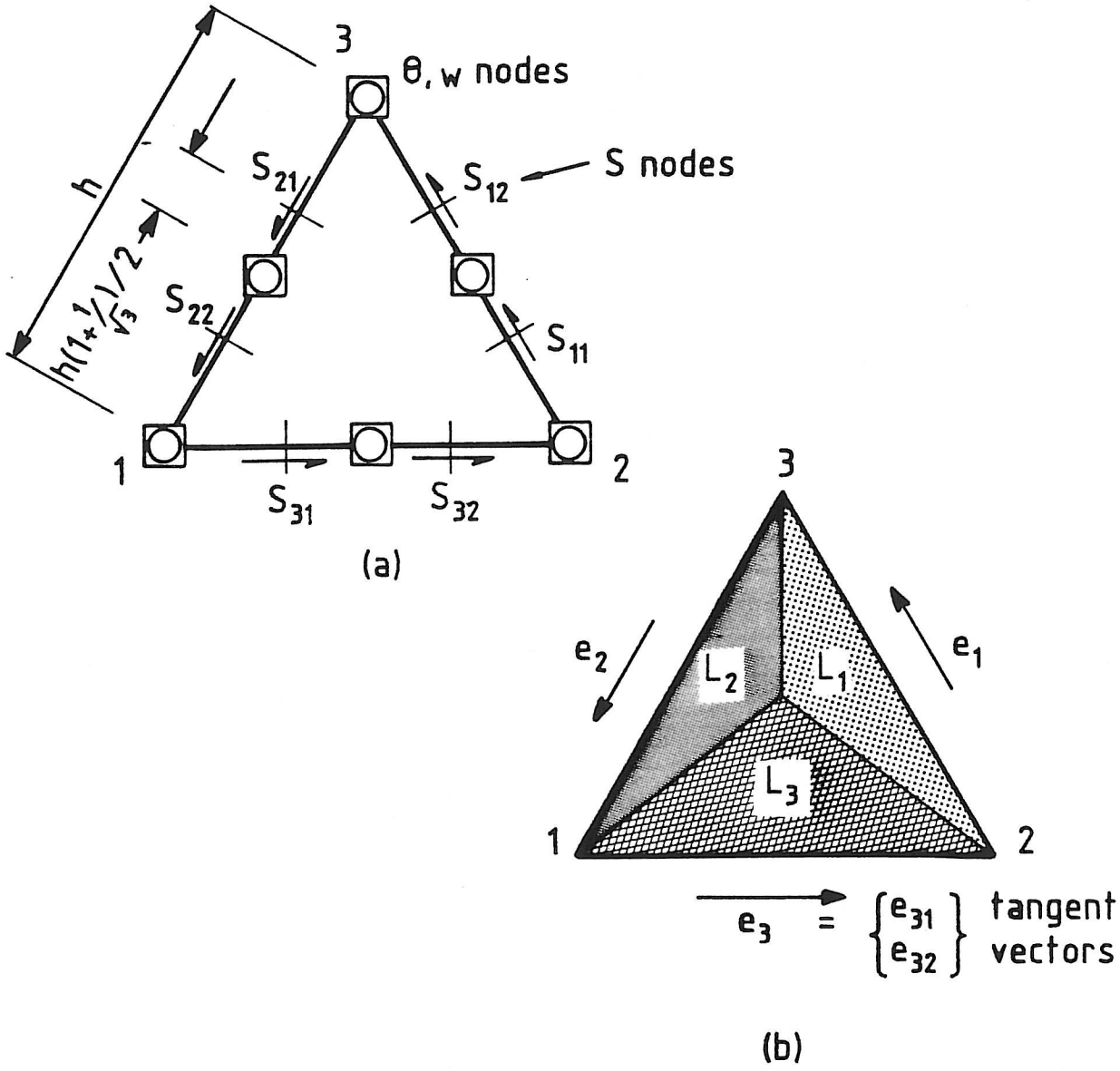

FIGURE 6 THE NEW QUADRATIC TRIANGULAR PLATE ELEMENT

(a) The parameters $\begin{pmatrix} \underset{\sim}{\theta} - 12 \text{ DOF} \\ \underset{\sim}{\Omega} - 6 \text{ DOF} \\ \underset{\sim}{S} - 6 \text{ DOF} \end{pmatrix}$

(b) Area co-ordinates and notation

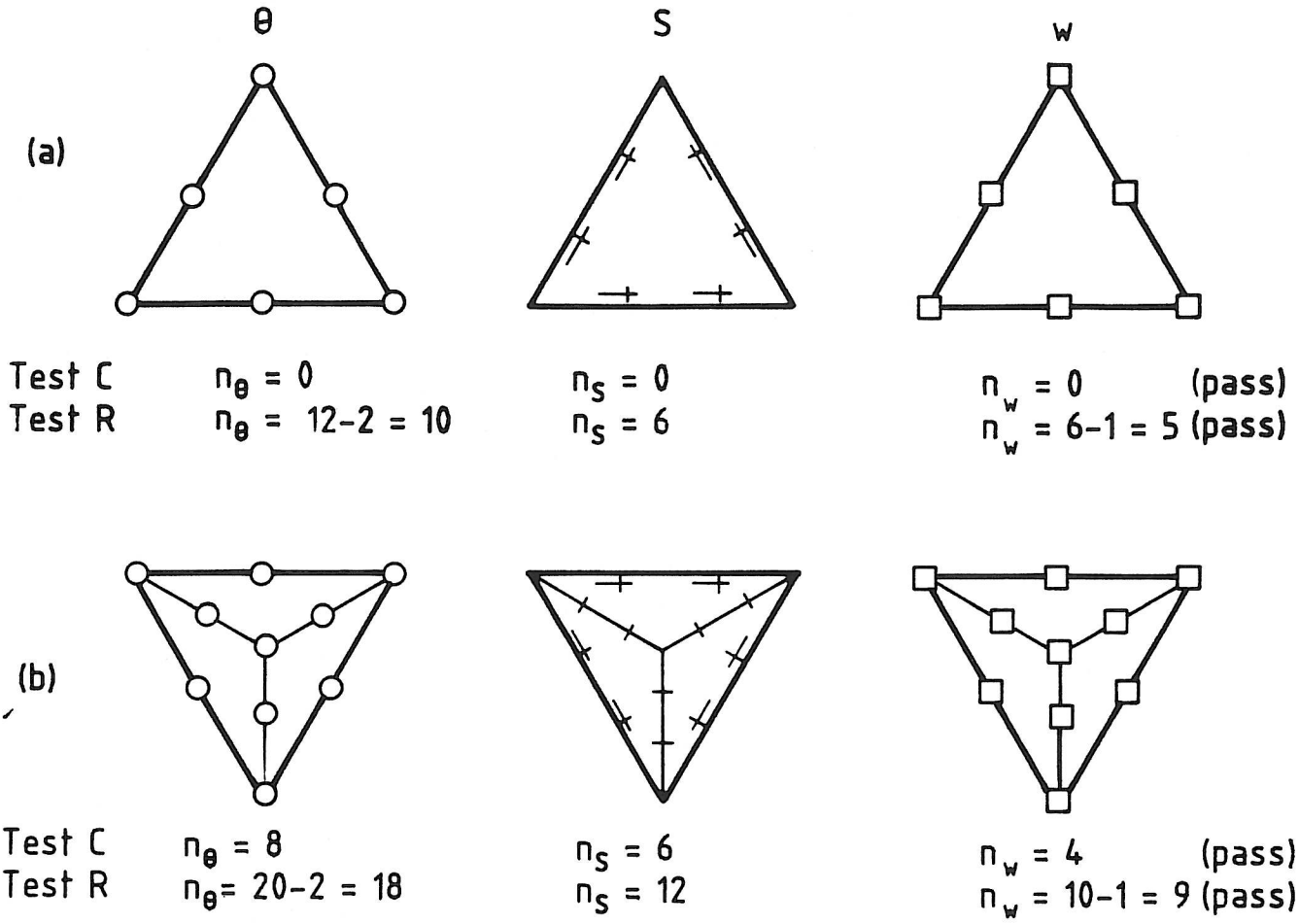

FIGURE 7 THE NEW QUADRATIC TRIANGULAR PLATE ELEMENT.
Patch count tests for single (a) and three element assemblies (b)

Note : This is a robust element as all patch tests passed

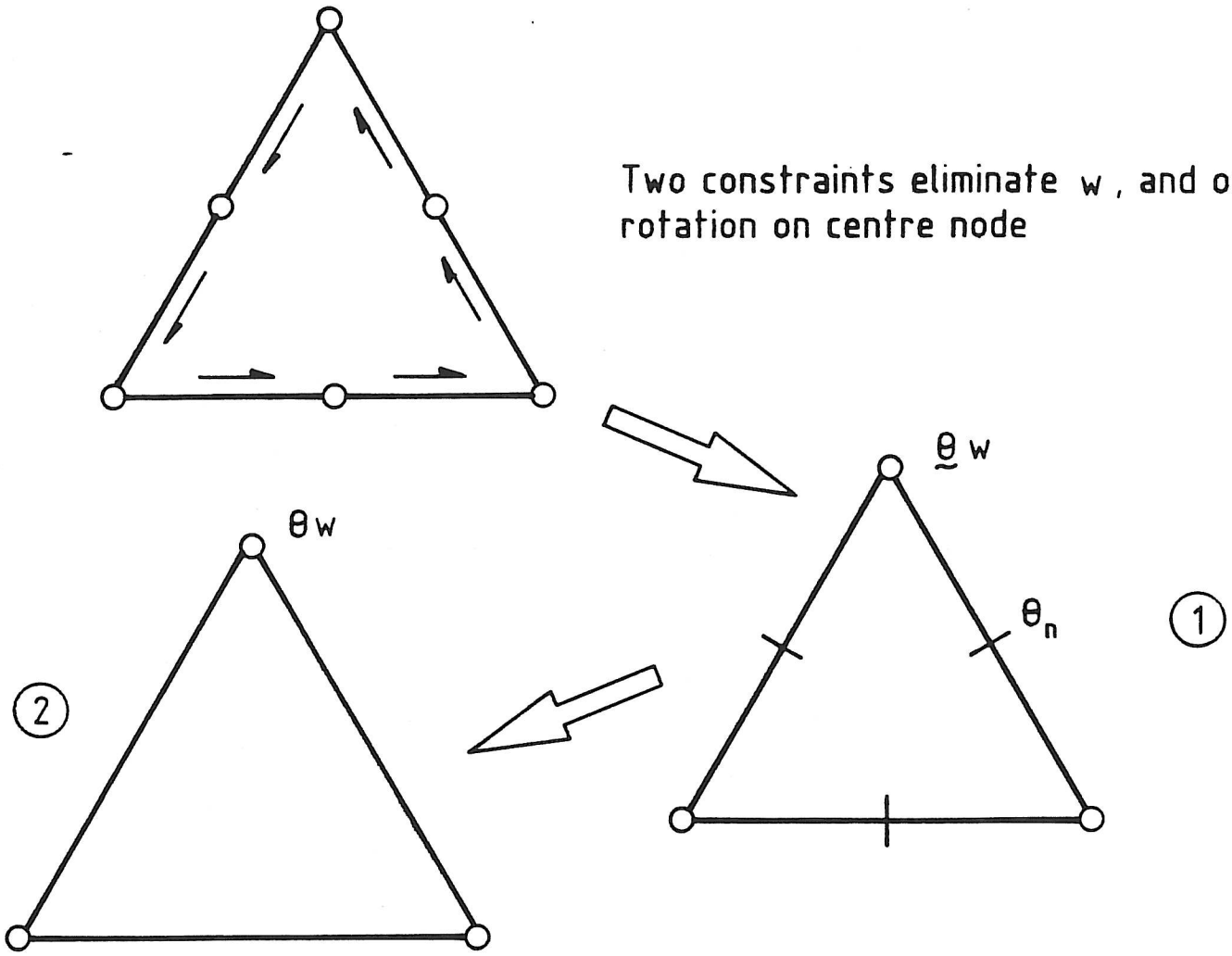

FIGURE 8 DEGENERATION OF THE NEW QUADRATIC TRIANGLE TO A DKT TYPE ELEMENT .

(1) with normal slopes prescribed at midsides . With an imposition of a further constraint requires the midside slopes to be the mean of those at corners.

The element (2) is obtained by transformation constraining θ_n to an average of nodal rotations

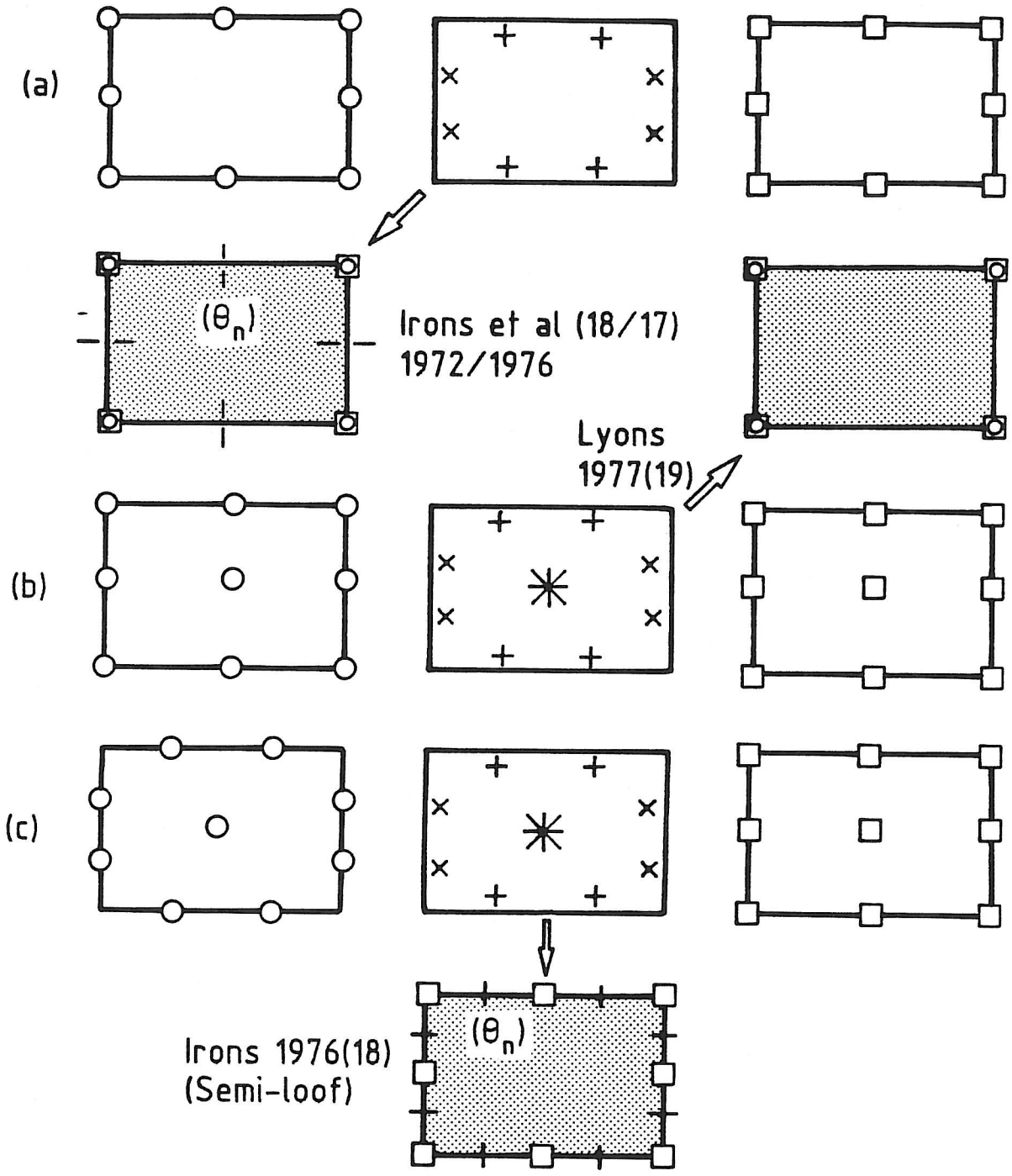

FIGURE 9 SOME POSSIBLE DISCRETE CONSTRAINT THICK PLATE ELEMENTS AND THEIR DKT EQUIVALENTS.
All elements pass the patch test count conditions

○ θ variables (2)
□ ω variables (1)
+ θ_n variables (1)

+ S_x } eliminated by
× S_y } discrete constraint

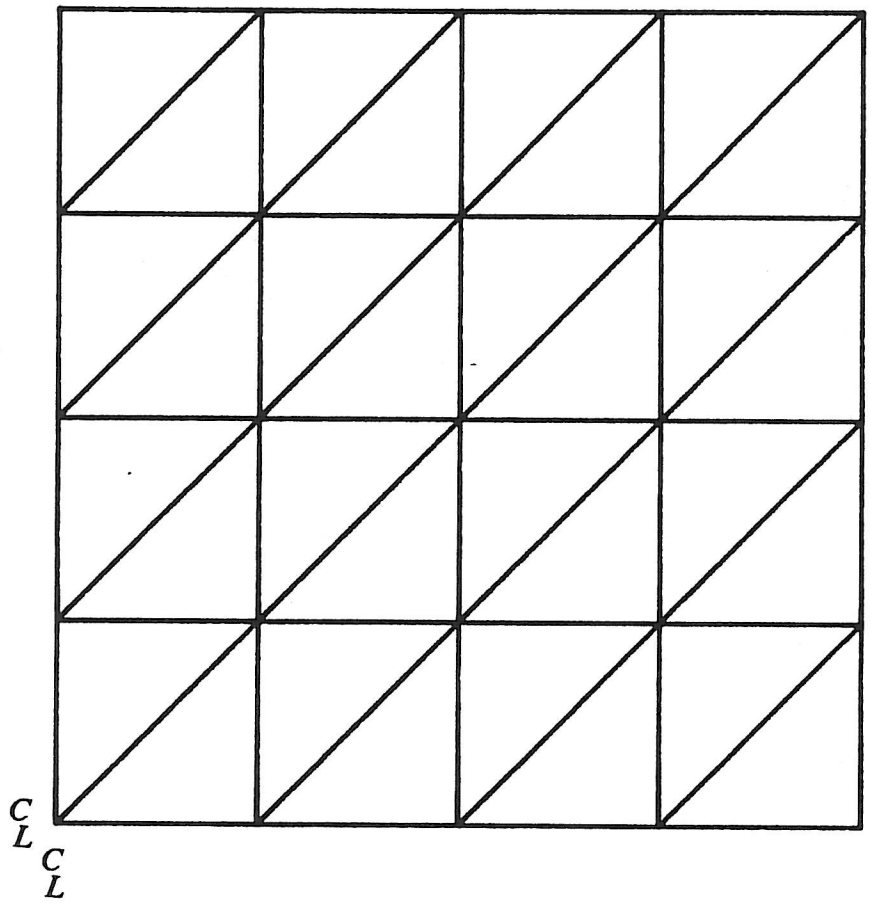

Mesh A

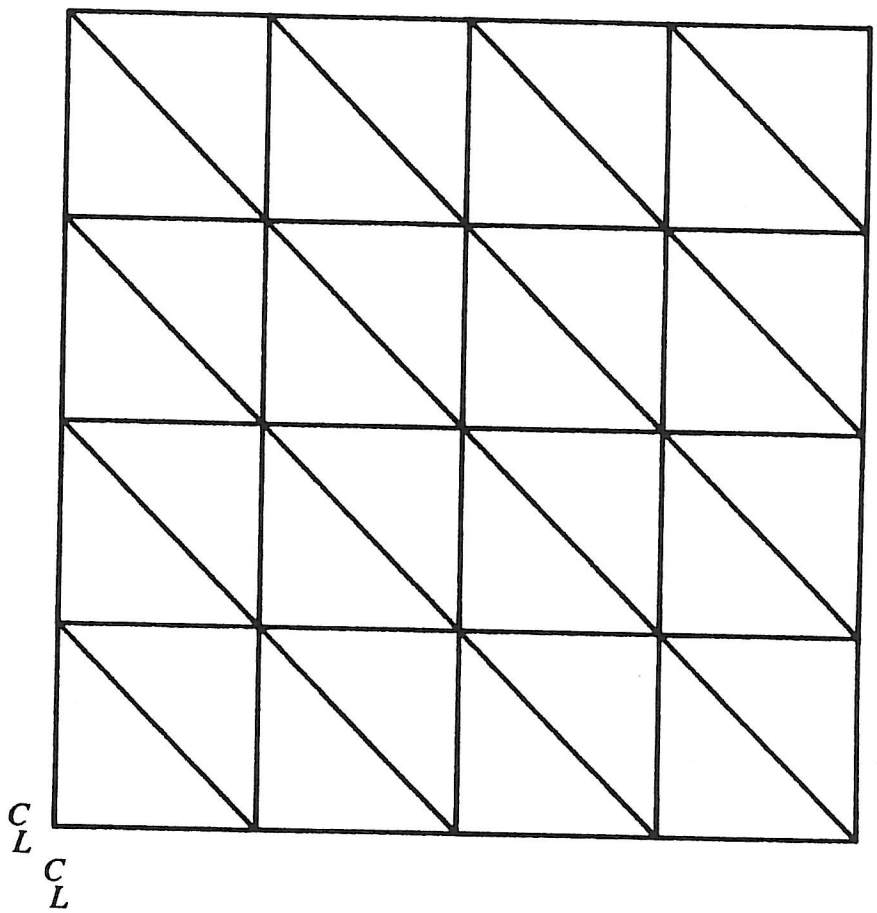

Mesh B

Figure 10. Mesh Types for Square Plates

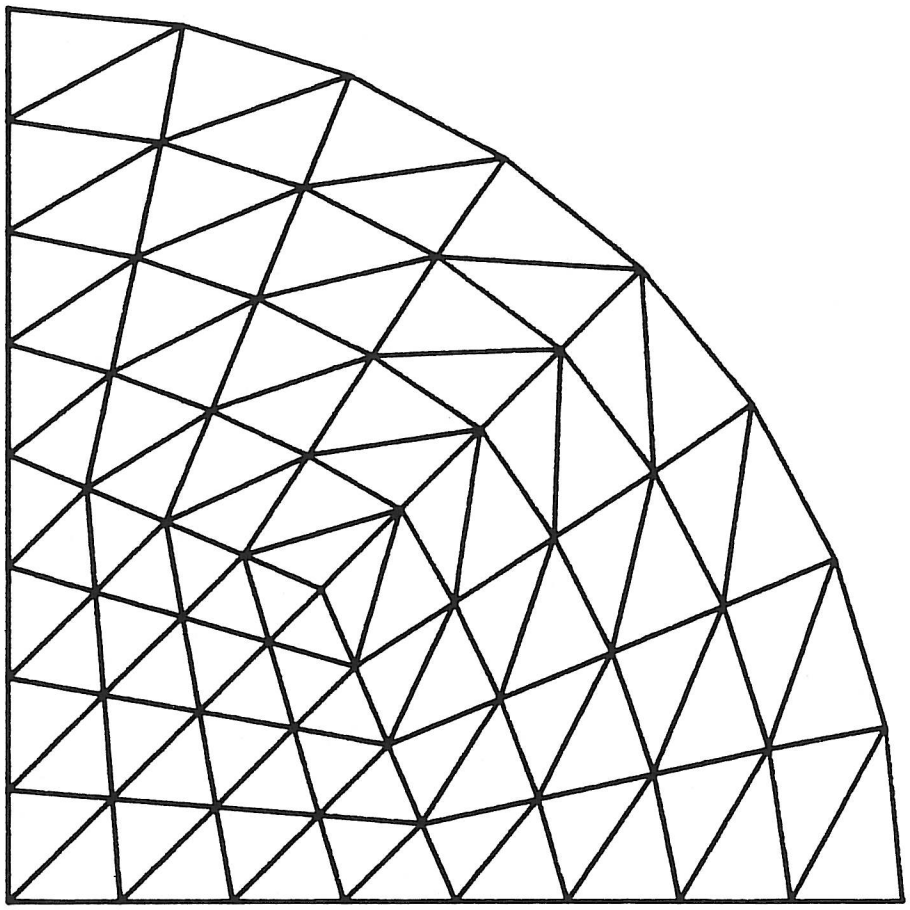

Figure 11. Typical Mesh for Quadrant of a Circular Plate - 96 Elements.

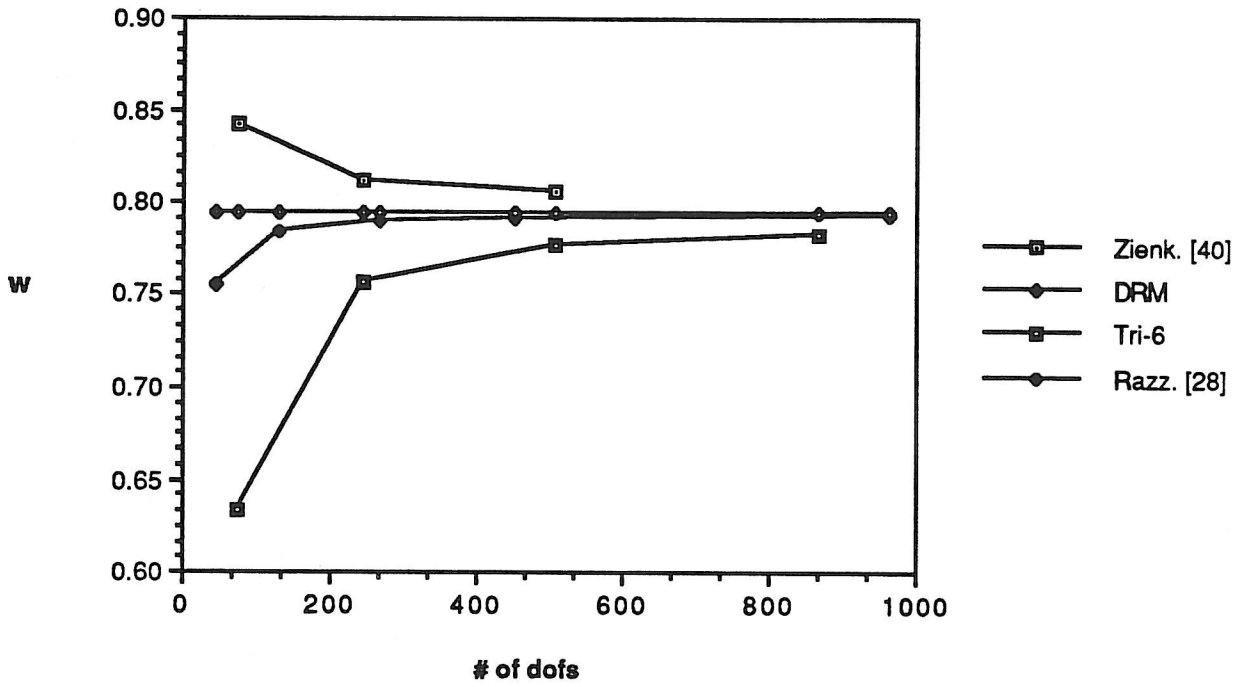

Figure 12. Convergence of Skew Plate Problem from Reference [40].

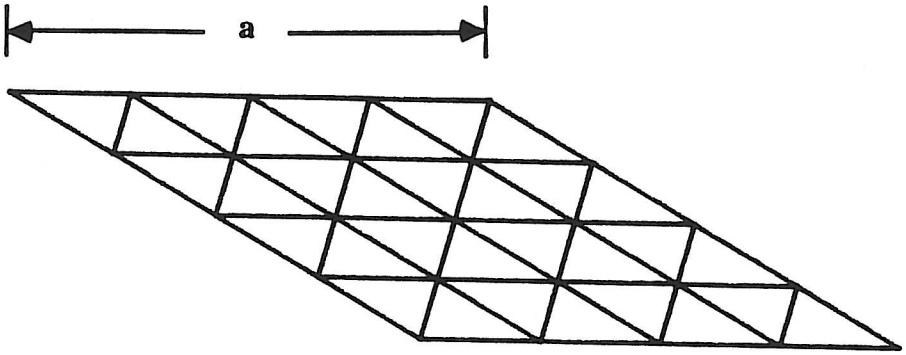

Figure 13. Typical Mesh for Morley Skew Plate Example.